Manuscript prepared for Atmos. Chem. Phys. Discuss.
with version 2014/09/16 7.15 Copernicus papers of the LaTeX class copernicus.cls.
Date: 4 February 2015

Dependence of the Vertical Distribution of Bromine Monoxide in the Lower Troposphere on Meteorological Factors such as Wind Speed and Stability

P. K. Peterson[1], W. R. Simpson[1], K. A. Pratt[2,*], P. B. Shepson[2,3], U. Frieß[4], J. Zielcke[4], U. Platt[4], S. J. Walsh[1], and S. V. Nghiem[5]

[1]Department of Chemistry and Biochemistry, Geophysical Institute, University of Alaska Fairbanks, Fairbanks, Alaska, USA
[2]Department of Chemistry, Purdue University, West Lafayette, Indiana, USA
[3]Department of Earth, Atmospheric and Planetary Sciences, Purdue University, West Lafayette, Indiana, USA
[4]Institute for Environmental Physics, University of Heidelberg, Germany
[5]Jet Propulsion Laboratory, California Institute of Technology, Pasadena, California, USA
[*]now at: Department of Chemistry and Department of Earth & Environmental Sciences, University of Michigan, Ann Arbor, Michigan, USA

Correspondence to: W. R. Simpson (wrsimpson@alaska.edu)

Abstract

Multiple axis differential absorption spectroscopy (MAX-DOAS) measurements of bromine monoxide (BrO) probed the vertical structure of halogen activation events during March–May 2012 at Barrow, Alaska. An analysis of the BrO averaging kernels and degrees of freedom obtained by optimal-estimation-based inversions from raw MAX-DOAS measurements reveals the information is best represented by reducing the retrieved BrO profile to two quantities, the integrated column from the surface through 200 m ($VCD_{200\,m}$), and the lower tropospheric vertical column density (LT-VCD), which represents the integrated column of BrO from the surface through 2 km. The percentage of lower-tropospheric BrO in the lowest 200 m was found to be highly variable ranging from shallow layer events, where BrO is present primarily in the lowest 200 m to distributed column events where BrO is observed at higher altitudes. The highest observed LT-VCD events occurred when BrO was distributed throughout the lower troposphere, rather than concentrated near the surface. Atmospheric stability in the lowest 200 m influenced the percentage of LT-VCD that is in the lowest 200 m, with inverted temperature structures having a first-to-third quartile range (Q1–Q3) of $VCD_{200\,m}$/LT-VCD from 15–39 % while near neutral temperature structures had a Q1–Q3 range of 7–13 %. Data from this campaign show no clear influence of wind speed on either lower-tropospheric bromine activation (LT-VCD) or the vertical distribution of BrO, while examination of seasonal trends and the temperature dependence of the vertical distribution supported the conclusion that the atmospheric stability affects the vertical distribution of BrO.

1 Introduction

The seasonal return of sunlight during late winter in the polar regions is associated with production of reactive halogens (e.g. Br, BrO, Cl) from saline ice surfaces (Abbatt et al., 2012; Saiz-Lopez and von Glasow, 2012). These halogen species influence boundary layer chemistry through phenomena such as boundary layer ozone depletion events (ODEs) (Barrie

et al., 1988; Simpson et al., 2007b) and mercury deposition events (MDEs) (Schroeder et al., 1998; Steffen et al., 2008). While the production mechanism of these halogens is not fully understood, modeling (e.g. Fan and Jacob, 1992; Mozurkewich, 1995; Lehrer et al., 2004; Piot and von Glasow, 2007; Yang et al., 2010; Parrella et al., 2012; Toyota et al., 2014), laboratory (e.g. Fickert et al., 1999; Huff and Abbatt, 2000; Wren et al., 2013) and field studies (e.g. Foster et al., 2001; Spicer et al., 2002; Toom-Sauntry and Barrie, 2002; Krnavek et al., 2012; Pratt et al., 2013; Liao et al., 2014) point to heterogeneous chemistry involving salts present on ice surfaces (e.g. NaBr, NaCl) as important sources of reactive halogens.

Multiple studies have examined the vertical extent of ODEs that result from halogen chemistry and have shown ODE vertical structure to be highly variable (Bottenheim et al., 2002b; Jones et al., 2010; Helmig et al., 2012; Oltmans et al., 2012). Jones et al. (2010) suggest a link between ozone depletion at higher altitudes and low pressure systems (storms) from Antarctic observations, but also point out that this relationship may not be the case in the Arctic due to differing meteorology. Ozonesonde data from ARCTAS/ARCPAC and OASIS campaigns presented in Oltmans et al. (2012) show the vertical extent of ozone depletion varies between 200 and 1000 m, and that this difference may be tied to the origin of the observed air masses in addition to the local meteorology. Although the profile of ozone depletion gives some insights into the vertical structures of the reactive halogens that deplete ozone, the differing chemical lifetimes of ozone (a day to longer) and reactive halogens (minutes to hour unless recycled by heterogeneous chemistry on particles) may mean that halogen vertical profiles differ from ozone depletion profiles. Tackett et al. (2007) present a view from tethered balloon measurements of a stratified lower boundary layer, in which the rates of ozone and Hg depeletion are determined by downward mixing into the halogen-chemistry-active surface layer. Moore et al. (2014) found that both ozone and mercury levels recovered to higher levels when vertical mixing induced by sea ice leads had recently influenced the observed airmasses, but the effect of this mixing on reactive halogens is not known. The work of Frieß et al. (2011) used MAX-DOAS observations along with optimal-estimation-based inversions to retrieve BrO concentration profiles and showed

significant variability in vertical structure with reactive halogens typically being in the lowest ~ 1 km of the atmosphere, similar to the ozone depleted layer.

The physical mechanisms for the transport of reactive halogens from the snow pack to the boundary layer and recycling of those halogens aloft are still poorly understood. Given the short lifetime of BrO in the absence of heterogeneous recycling (McConnell et al., 1992; Platt and Hönninger, 2003), it is likely that some sort of aerosol particles (Fan and Jacob, 1992), either from blowing snow or other sources are required to sustain halogen activation aloft. Recent literature in particular has focused on the role of blowing snow events in halogen activation (e.g. Jones et al., 2009, 2010; Yang et al., 2010; Frieß et al., 2011). In particular, Jones et al. (2009) used O_3 observations at Halley station in Antarctica, to derive a model for the dependence of ODEs on wind speed. Jones et al. (2009) suggest that there are two environmental regimes that favor local halogen activation and subsequent ozone depletion. One regime consists of low wind speeds and a stable boundary layer, the other requires high winds and the presence of blowing snow. Blowing snow events occur when high winds loft snow, potentially enhancing available snow surface area available for reaction. Blowing snow may shift reactive halogens aloft through reactions on the blowing snow or aerosol particles produced by sublimed blowing snow (Jones et al., 2009, 2010; Yang et al., 2010; Frieß et al., 2011). Comparison of satellite-observed column BrO data with modeling results by Yang et al. (2010) suggests that blowing snow events may be sufficient to explain the majority of halogen activation events observed via satellite. In contrast, Halfacre et al. (2014) conducted an analysis at a variety of locations across the Arctic and found no relationship between observed ozone and wind speed, suggesting that high wind speeds, and consequently blowing snow, may not play a major role in ozone depletion. Again, because of the differing chemical lifetimes of ozone and reactive halogens, using ozone depletion as a proxy for halogen activation requires caution.

To examine these ideas further, it is necessary to observe both the total amount of reactive halogens, and their distribution throughout the lower troposphere. While satellite measurements (e.g. Wagner and Platt, 1998; Richter et al., 1998; Chance, 1998) provide extensive spatial coverage of the Arctic, they only measure the total column of BrO, and do

not provide vertical profile or near surface information. Multiple methods exist to separate total column measurements into stratospheric and tropospheric components (e.g. Theys et al., 2011; Salawitch et al., 2010; Koo et al., 2012; Sihler et al., 2012). However, discrepancies still exist between ground based and satellite based measurements, potentially due to clouds masking portions of the tropospheric BrO column from satellite views. Additionally, Theys et al. (2009) and Salawitch et al. (2010) showed that some of the variability of total column BrO arises from stratospheric variability, thus not all satellite-detected BrO "hotspots" are actually lower tropospheric halogen activation events. In-situ chemical ionization mass spectrometry (e.g. Liao et al., 2011; Pratt et al., 2013; Liao et al., 2014) and long path differential optical absorption spectroscopy (LP-DOAS) (e.g. Tuckermann et al., 1997; Pöhler et al., 2010) fail to capture the vertical extent of halogen activation, except in the case of limited aircraft-based campaigns (e.g. Neuman et al., 2010; Liao et al., 2012), and thus can not address questions about the total amount of halogen activation taking place at a given time. However, the Tackett et al. (2007) work implied that much of the halogen chemistry is occurring in the lowest $\sim 200\,\mathrm{m}$ of the boundary layer.

Multiple axis differential optical absorption spectroscopy (MAX-DOAS) has the ability to retrieve vertical profiles of BrO in the lowest few kilometers, and thus can examine the variability of the vertical distribution of BrO over time (Frieß et al., 2011). The present work builds on the method of Frieß et al. (2011) by considering the BrO averaging kernels, which provide information on the sensitivity of these BrO measurements (Payne et al., 2009), to identify what observations are independent of the a priori assumed profile of BrO and creating a consistent timeseries of these data over a field campaign. Through this analysis, we identify two relevant properties of the BrO vertical profile, the partial vertical column density (VCD) of BrO in the lowest 200 m (termed $\mathrm{VCD}_{200\,\mathrm{m}}$) and the lower-tropospheric partial VCD (termed LT-VCD). The present work explores the dependence of these BrO profile properties on environmental factors to investigate activation of BrO and its propagation outside of the near surface layer over time. This present work focuses on measurements occurring near Barrow, Alaska, during the Bromine, Ozone, and Mercury Experiment (BROMEX) campaign (Nghiem et al., 2013) from 6 March to 15 May 2012. The primary MAX-DOAS

observations were made from the roof of the Barrow Arctic Research Center (BARC) building at 71.325° N, 156.668° W, which is about 6 km northeast of the city of Barrow, Alaska, with a viewing azimuth of 27 degrees east of true north.

2 Methods

2.1 MAX-DOAS measurements

Multiple-Axis Differential Optical Absorption Spectroscopy (MAX-DOAS) probes vertical distributions of trace gases above a measurement site through a combination of spectroscopic measurements of scattered sunlight and modeling of vertical profiles consistent with those observations (Hönninger et al., 2004). The instrument measures spectra of scattered sunlight in a region where the molecule of interest absorbs as a function of elevation angle of a telescope receiving the light. Measurements at all elevation angles contain absorption features due to stratospheric and higher tropospheric gases, and because most sunlight is scattered in the lower atmosphere, these stratospheric absorption features are common to observations at all elevation angles. Measurements at low elevation angles contain enhanced absorption for gases present near the ground, due to the tangent geometry of the light's final path to enter the telescope at a low elevation. Therefore, analysis of the relative absorption spectrum comparing light at low elevation angles to high elevation angles provides high sensitivity to near-ground absorbers with greatly reduced sensitivity to stratospheric and upper tropospheric gases.

The instrument used in this study is similar to the one described in Carlson et al. (2010) with a few improvements. In this study, we measured scattered sunlight using a QE-65000 (Ocean Optics) spectrometer with spectral range from 309–397 nm and optical resolution of 0.39 nm full width at half maximum. This new spectrometer is improved by using a thermoelectrically cooled detector, stabilized at $-15\,^{\circ}$C. The spectrometer optical bench is heated to 38 °C, with a standard deviation of 0.6 degrees over the full campaign, to improve optical alignment stability. Another improvement of the instrument is the use of a MEMS tiltmeter

(SignalQuest SQ-SI-360DA-3.3R-HMP-HP-IND-S) mounted on the moving telescope that directly measures the elevation angle of the observation. The scan pattern measures scattered sunlight at elevation angles of 90° (zenith), 20°, 10°, 5°, 2°, and 1° over a period of approximately 30 min.

We used QDOAS software (Fayt et al., 2011) to fit the relative absorption spectrum between near temporally coincident low elevation and zenith observations to a linear combination of possible absorbing spectra to quantify the differential slant column density (dSCD) of each absorbing gas at each elevation angle. We performed this analysis in the wavelength window between 346 and 364 nm. The absorber cross sections are detailed in Table 1 and are convoluted with an instrumental transfer function measured from the 334 nm line of a low pressure mercury lamp. In addition to gaseous absorbers, we include a third-order polynomial to account for Rayleigh and Mie scattering by gases and particles in the atmosphere, and a spectral offset to account for stray light within the spectrometer. The mean residual root mean square (RMS) of our dSCD retrieval was 3.9×10^{-4}. Data collected during low sight conditions (solar zenith angle $> 85°$), RMS $> 10^{-3}$, or when frost is detected on the instrument's optical window are discarded. The dSCD fitting errors (1σ) over the campaign average 1.9×10^{13} molecules cm^{-2} for BrO and 5.1×10^{41} molecules^2 cm^{-5} for O_4. The sensitivity of the RMS and dSCD errors to elevation angle was small (< 15%) and is documented in the supplemental material.

2.2 Retrieval of vertical profiles

Retrieval of trace gas vertical profiles from dSCD data is a two-step procedure. First, we determine the aerosol particle extinction vertical profile from O_2 collisional dimer (O_4) dSCD measurements using an optimal estimation procedure detailed in Frieß et al. (2006) and briefly described here. The observed O_4 dSCD values are strongly dependent on atmospheric visibility and light scattering, which we are able to deduce because we know the vertical profile of O_4. Measured O_4 dSCDs are compared to values modeled using the SCIATRAN radiative transfer model (Rozanov et al., 2005), which depend on a variable aerosol particle extinction profile and static parameters such as the viewing geometry and aerosol

particle light scattering properties. Assumptions made about the aerosol optical properties are set to values typical for clean ice crystals, following the procedures detailed in Frieß et al. (2011). Because the measured O_4 data alone do not provide enough information to retrieve the profile, we used an assumed a priori profile to further constrain the solution, as described by Rodgers (2000). We used a variable a priori profile that peaks at the surface and exponentially decays with altitude. Initially, the profile peaks at the surface with an aerosol particle extinction value of $0.05\,km^{-1}$ and exponentially decays with a scale height of 1 km. The initial a priori covariance matrix is constructed with the diagonal elements being the square root of 3 times the a priori extinction and the off-diagonal elements being set to 0. The a priori covariance matrix is changed with every iteration (Frieß et al., 2006). In following iterations, the a priori is set to the retrieved profile and smoothed using a boxcar average with a width of 300 m (Frieß et al., 2006). The final output of this first step is a vertical profile of aerosol particle extinction.

The procedure to retrieve the BrO profile from BrO dSCD measurements is described in detail in Frieß et al. (2011). Briefly, we used the above-retrieved aerosol particle extinction profiles as input to a Monte Carlo radiative transfer model (McArtim, Deutschmann et al., 2011) that simulates BrO dSCDs as a function of a variable BrO vertical concentration profile. The vertical profile of BrO is varied to give best fit to the BrO dSCD observations, again by optimal estimation. In the case of BrO, the a priori profile peaks at the surface with a value of $10\,pmol\,mol^{-1}$ and exponentially decays with a scale height of 400 m. The result of the second step is the average BrO mixing ratio every 100 m from the ground to an altitude of two kilometers. An example of the retrieved profile is shown in green in Fig. 1. Note that while our general retrieval uses a 400 m scale height for the a priori profile of BrO, Fig. 1 also includes the effect of modifying the a priori profile to have a different (1000 m) scale height (dashed blue line), as described below.

2.3 Information content of the profile

The retrieved BrO profiles contain average mixing ratios in twenty 100 m thick layers from the surface to 2 km; however, they are based on only five low-elevation spectral measure-

ments of BrO dSCD. Therefore, it is clear that our observations contain less information about the true vertical profile than is represented in Fig. 1. The optimal estimation method used the assumed a priori information to constrain the fit in the absence of further information, but the actual vertical profile of BrO is not known. In fact, the results of this study indicate that both the BrO abundance and vertical profile shape vary over time. Therefore, the full profile, as retrieved by optimal estimation, lends itself to overinterpretation of the observations and we seek to find a method to determine the actual information content, as well as reduce the number of derived properties to reflect the true observations more accurately.

As described in Rodgers (2000), the retrieved profile contains true profile information as well as a bias toward the assumed a priori profile. The extent to which the retrieved profile depends on the dSCD measurement data is determined by examining the averaging kernel matrix. An example of the BrO averaging kernels for a MAX-DOAS retrieval is given in the left panel of Fig. 2. If the value of the diagonal element of the averaging kernel at some altitude were unity (1), it would indicate that all of the information content at that layer is constrained by observational data and none of the information at that altitude comes from the a priori assumption. Non-zero off-diagonal elements indicate that the retrieved parameter in that layer is not independently resolved and is influenced by results in other layers. There are two peaks in the averaging kernels, one at the surface and one aloft at an altitude of about 300 m. We can understand the sharp peak at the surface easily because MAX-DOAS spectroscopy always has highest sensitivity and greatest vertical resolution in the layer in which the observer resides. In this study, that is the lowest portion of the boundary layer when the measured photons traverse a path tangent to the ground prior to being detected. The broader peak aloft, centered at about 300 m, in this example, comes from the observations at higher elevation angles, which view through those aloft layers, but do not provide enough information to independently resolve mixing ratios in 100 m thick layers at higher altitudes. The trace (sum of diagonal elements) of the averaging kernel matrix gives the degrees of freedom (DOF), which represents the total number of independent pieces of information contained in the retrieval. For BrO retrieval using this technique and our in-

strumentation, the distribution of DOF is well fit by a Gaussian function, with a mean of 2.0 DOF and $\sigma = 0.27$. Our retrievals also exhibit a distinct lack of sensitivity to changes in individual 100 m layers at altitudes over 1000 m. The DOF for this example is 1.99, implying our retrieved profile contains two independent pieces of information, rather than the 20 we retrieved.

To illustrate the influence of our a priori assumptions, Fig. 1 also shows a retrieved profile with a different assumed BrO scale height, 1000 m instead of the normal 400 m assumption. The influence of a priori selection in the retrieved BrO mixing ratio in the lowest 200 m is minimal, showing that our instrument is most independent of a priori assumptions about the BrO profile near the surface. However, aloft the effects of a priori selection are clearly visible. What appeared to be a relatively sharp peak at ≈ 650 m when the 400 m a priori was assumed becomes much broader with the 1000 m assumed scale height. Note that both optimally estimated results fit the observational data with similar figure of merit (χ^2), so the difference in profile is not due to poor fitting in one case or the other, but instead a consequence of the a priori influencing the resultant BrO profile.

2.4 Reduction of the full profile

A method for mapping the BrO profile retrieved on a fine grid to a course grid, such that the DOF are represented as physical quantities without the influence of a priori information is outlined in von Clarmann and Grabowski (2007). They suggest moving to a variable coarse altitude grid where one would select grid points such that each grid point would represent one DOF. The lowest layer's upper boundary would be determined by summing the diagonal elements of the BrO averaging kernel matrix until the sum reached one. This process would be repeated to obtain additional layer boundary altitudes. However, this approach is not practical for long-term time series analysis because the vertical resolution would vary over time, making comparisons difficult. As a compromise, we calculated coarse grid points by examining the ensemble of profile retrievals over this campaign and splitting them into two layers by determining the average altitudes such that each layer contains one degree of freedom. This method led us to represent one degree of freedom as the abundance of

BrO from surface through 200 m, and another as the abundance of BrO from 200 m to 2.0 km. These two layers differ in thickness due to the enhanced vertical resolution at the surface and decreased vertical resolution aloft, so we choose to represent the abundance in each layer is a partial vertical column density (VCD) within each layer. The vertical column density is also useful because satellite total column retrievals of BrO use the same unit of abundance. Thus, our two quantities ($VCD_{200\,m}$ and VCD_{Aloft}) represent a surface layer VCD and a lofted layer VCD respectively.

Figure 1 shows the partial VCDs in each layer derived from the grid coarsening procedure, for an example retrieval. While the profiles look fairly different, particularly aloft, the partial VCDs in each of the layers are only around ten percent different from each other as an effect of the assumed a priori profile. This example shows how the grid coarsening procedure gives results that are less dependent on the unknown but assumed BrO profile.

Payne et al. (2009) describe how to calculate general averaging kernels for a coarsened grid, which we applied to our BrO retrievals. An example of the coarse grid BrO averaging kernels is shown in Fig. 2. The DOF has been reduced, meaning we have lost some information in the transfer to a coarse grid, however, both parameters have averaging kernels that peak within the desired layer and at a value close to unity, implying most of the information comes from the observations. Payne et al. (2009) suggested a cutoff of 0.7 for the diagonal element of the averaging kernel within a layer as sufficiently close to unity to consider the observations as derived from the data and independent of the a priori assumption. We chose to adopt the same cutoff of 0.7 degrees of freedom in the present work.

The right panel of Fig. 3 shows the dependence of the aloft information content on the aerosol optical depth. As Fig. 3 shows, our ability to retrieve information beyond the near surface layer is heavily dependent on the aerosol optical depth, while our ability to retrieve information near the surface is less influenced by aerosol particles. In addition to the degrees of freedom cutoff, over the course of the campaign we also observed limited times when the retrieved aerosol optical depth was large, in excess of 2, which indicates that the visibility is insufficient to obtain an accurate profile of aerosol particle extinction or BrO. During these periods, we do not consider the VCD_{Aloft} due to insufficient degrees of freedom,

and we also disregard the $VCD_{200\,m}$. This approach is consistent with methods used in comparison of near-surface MAX-DOAS and LP-DOAS BrO measurements by Frieß et al. (2011).

When both quantities have averaging kernels peaking at 0.7 or higher, we refer to the sum as the lower tropospheric vertical column density (LT-VCD). It is important to note that this quantity does not represent a new degree of freedom, as it is derived from and not independent of the other two measurements. To evaluate the vertical distribution of BrO, we examine the ratio of the $VCD_{200\,m}$/LT-VCD as well as the total amount of observed activation in the lower tropospheric (LT-VCD) and near surface amounts ($VCD_{200\,m}$). A time series of these three quantities, along with the aerosol optical depth over a portion of the campaign is presented in Fig. 4. The rest of the timeseries can be found in the supplemental material. This timeseries will be discussed below, but here we note that the fraction of BrO in the lower layer varies between a few percent and up to $\approx 80\,\%$. The a priori profile, exponentially decaying with a scale height of 400 m, would have a constant fraction of BrO in the lowest 200 m, approximately 34 %. It is clear that the data show substantially more vertical profile variability than the assumed profile. Therefore, we use the grid-coarsened data to represent the information content from our MAX-DOAS observations over this long time period.

An additional advantage of the coarsened grid is that the resulting quantities are less sensitive to errors in forward model parameters. As an example, the aerosol particle extinction profile required for the BrO retrieval is also an optimally estimated quantity, and not the true profile. This will introduce errors in the BrO retrieval. We estimated the errors in BrO retrieval due to uncertainties in the aerosol particle extinction profile by examining the sensitivity of the BrO retrieval to perturbations in the aerosol particle extinction profile. To do so, we retrieved BrO profiles from the same BrO dSCD data over an ensemble of varying aerosol particle extinction profiles observed during this study, and examined the resulting variability in the quantities further discussed in this manuscript. We found that the LT-VCD was not heavily influenced by changes in the aerosol profile, with an estimated error of 4.6% (1 σ), which is lower than error introduced by uncertainties in the BrO dSCD measurements. The VCD_{200m}/LT-VCD ratios retrieved have an estimated error of 4.9% (1

σ). Thus, it is reasonable to conclude that the vertical structure of halogen events retrieved using MAX-DOAS at Barrow is not substantially influenced by errors in aerosol retrieval.

2.5 Other field sites

Figure 5 shows locations for various measurements used in this study. While this paper focuses on MAX-DOAS measurements from the BARC building, Sect. 3.3 makes use of data from multiple field sites to evaluate the effectiveness of our near-surface BrO retrieval. We deployed a second MAX-DOAS instrument, IL1, at 71.355° N, 155.668° W, which is on landfast sea ice east of the BARC building with a viewing azimuth of 2 degrees east of true north. This instrument is the same as the instrument on the BARC building, with the exception of the spectrometer, which is an Avantes (AvaSpec-ULS2048x64-USB2) with spectral range from 291–457 nm and optical resolution of 0.37 nm full width at half maximum. This spectrometer is housed in a highly insulated enclosure that is stabilized at 10 °C using air cooling. We analysed MAX-DOAS data from IL1 using the techniques previously described. For IL1, the mean RMS of our dSCD retrieval is 5.2×10^{-4}. IL1 dSCD fitting errors (1σ) over the campaign average 9.7×10^{12} molecules cm^{-2} for BrO and 1.7×10^{42} molecules^2 cm^{-5} for O_4 .

Additional surface BrO measurements were conducted near Barrow, AK from 12–28 March 2012 at a measurement site about 5 km inland (71.275° N, 156.641° W), shown in Fig. 5, using a chemical ionization mass spectrometer (CIMS), described by Liao et al. (2011). Using hydrated $I^-(I \cdot (H_2O)_n^-)$ as the reagent ion, BrO was measured at mass 222 ($I^{79}BrO^-$) and 224 ($I^{81}BrO^-$). Background measurements were performed every 15 min by passing the air flow through a glass wool scrubber. Br_2 calibrations were performed every two hours by adding Br_2, from a permeation source, in 21 mL min^{-1} N_2 to the air flow. A relative sensitivity of BrO (mass 224) relative to Br_2 (mass 287) of 0.47 was utilized for BrO calibration (Liao et al., 2011). The presence of BrO was confirmed by the ratio of mass 222/mass 224 (background-subtracted raw signals), calculated to be 1.01 ($R^2 = 0.94$).

For a measurement cycle of 10.6 s, mass 224 ($I^{81}BrO^-$) was monitored for 0.5 s, giving a 5 % duty cycle. The 3σ limit of detection for BrO, using mass 224, was calculated

to be 1.6 pmol mol^{-1}, on average for a 2.8 s integration period (corresponding to 1 min of CIMS measurements). Since the variance in the background is likely due to counting statistics (Liao et al., 2011), the limit of detection for 30 min averaging is estimated at 0.3 pmol mol^{-1}. The uncertainty in the reported BrO concentrations was calculated to be $30\% + 0.3$ pmol mol^{-1}. Additional sampling details are provided in the Supplementary Information.

To examine relationships between BrO and ozone, as well as local meteorology, we used ozone data and meteorological data from the National Oceanic and Atmospheric Administration (NOAA) Earth Systems Research Laboratory/Global Monitoring Division (ESRL/GMD). These data included near surface ozone mixing ratios, temperature, wind speed, wind direction, pressure, as well as twice daily meteorological balloon sounding data from the Barrow Airport (PABR), which was used to calculate the temperature gradient (dT /dz) near the surface. These soundings take place twice daily, at 00:00 UTC, which is in the daylight hours, 15:00 AKST, at Barrow, and 12:00 UTC, which is at night and not used in this study.

3 Results

3.1 Relationship between visibility and retrieval information content

The ability of MAX-DOAS to observe BrO beyond the near surface layer is heavily influenced by the optical properties of the atmosphere (e.g. visibility) at the time of the measurement. The methods outlined above allow us to identify times when MAX-DOAS measurements are sensitive to BrO beyond the near surface layer and restrict our further analysis of the vertical distribution of BrO to these periods. Figure 3 details the relationship between the aerosol optical depth and the information content of the measurement. As the aerosol optical depth increases, the ability to observe the full LT-VCD sharply decreases. As seen in Fig. 3, we can retrieve the full LT-VCD 50 % of the time. We excluded periods where we

are unable to fully observe the LT-VCD from further analysis of the vertical distribution of BrO.

3.2 Influence of ozone

Ambient ozone levels influence the partitioning of reactive halogen species between atomic (e.g. Br atoms) and oxide (e.g. BrO) forms. MAX-DOAS measurements retrieve only BrO and thus only constrain one component of BrO_x ($BrO + Br$). Therefore, it is important to consider effects of gas-phase partitioning of BrO_x on subsequent conclusions about halogen activation. Under ordinary ozone conditions (ozone mixing ratios of 30–40 $\mathrm{nmol\,mol^{-1}}$), BrO will make up the majority of BrO_x; however, as ozone levels approach zero (a common occurrence during the ozone depletion event season), our BrO-only measurements could be insufficent to observe reactive halogens, as shown in Helmig et al. (2012). We term this effect "ozone titration" and seek to avoid interpretation of BrO data below some threshold where the effect dominates. The threshold depends on the photolysis rate of BrO, which varies depending on cloud cover and solar zenith angle, among other factors. For the purposes of this study, we used an ozone threshold of $< 1\,\mathrm{nmol\,mol^{-1}}$ to identify potentially titrated air masses to exclude from further analysis (Simpson et al., 2007a). Figure 4 shows times when ozone is below $1\,\mathrm{nmol\,mol^{-1}}$ as shaded in grey. Note that, for the most part, BrO LT-VCD and $VCD_{200\,m}$ are small during ozone titration, as would be expected, and also observed by Neuman et al. (2010).

3.3 Influence of airmass history

Airmass history, particularly time spent in sea ice areas, can influence observed BrO at coastal sites (e.g Frieß, 2004; Simpson et al., 2007a). To examine the variability in airmass history during BROMEX, we calculated time spent in sea ice areas over the 72 hours prior to each measurement using methods detailed in Simpson et al. (2007a). During BROMEX, all measured airmasses spent at least 25% of the past 72 hours in contact with sea ice while 90% of measured air masses spent over 75% of the past 72 hours over sea ice. While

there is an influence of airmass history on the observed BrO, given the high levels of sea ice contact observed throughout the campaign, it is unlikely that the variability of BrO observed during this campaign can be attributed to variations in air mass history.

3.4 Performance of surface BrO retrieval

To evaluate the effectiveness of the BrO retrieval near the surface, we used in situ BrO measurements made using chemical ionization mass spectrometry (CIMS) to evaluate our retrieval in the lowest 100 m. While the mixing ratio in the lowest 100 m is not one of the grid coarsened quantities, because MAX-DOAS is most sensitive near the surface, the near surface mixing ratio has similar information content to the $VCD_{200\,m}$ while minimizing the effects of vertical averaging on comparison with in situ measurements. Figure 6, shows a timeseries of the average BrO mixing ratio retrieved in the lowest 100 m by MAX-DOAS (Red) and in situ CIMS measurements taken 1 m above the snow pack (Green). The error associated with 100 m mixing ratios retrieved using MAX-DOAS varies depending on the state of the atmosphere at the time of the measurement. The error associated with each retrieval is determined by examining the sensitivity of the retrieval to dSCD errors associated with the measurement data (Rodgers, 2000). Average errors (2σ) were 4.2 pmol mol^{-1} for our MAX-DOAS measurements. Uncertainties are estimated at $30\,\% + 0.3$ pmol mol^{-1} for CIMS measurements. Because the CIMS instrument was also used to conduct snow chamber experiments during BROMEX, and MAX-DOAS observations are daytime only, there are some gaps in the timeseries shown in Fig. 6.

Because CIMS measures in one discrete location just above the snowpack, while MAX-DOAS measurements are spatially averaged, both horizontally over 10–20 km and vertically over approximately 100 m, it is expected that large changes in the environment in the view direction of the MAX-DOAS will cause differences between the CIMS and MAX-DOAS observations. We also expect that because the snowpack is a source of Br_2 (Pratt et al., 2013), there may be a significant near-surface BrO gradient. Figure 6 shows a time series of near surface BrO measurements from the CIMS, as well as MAX-DOAS measurements at the BARC building. Since the BARC data originate at ~ 4 m, and average over the lowest

100 m, we might expect MAX-DOAS data to be lower than the CIMS, which measures closer to the snowpack. Figure 6 shows agreement for the majority of concurrent observations, excluding the period shaded in gray, during which we observed substantial gradients in the near surface amounts of BrO at IL1 (blue line) and BARC (red line), which could explain discrepancies between the MAX-DOAS measurements at the BARC building and the CIMS measurements. Figure 5 shows the MAX-DOAS instrument on the BARC building views across a large lead that is not sampled by the IL1 view direction, which could potentially explain a local gradient in BrO. Figure 7 shows the overall correlation between MAX-DOAS measurements at the BARC building and the CIMS, each averaged to hourly bins. Points occurring during the gray period marked on Fig. 6 are shown in red open circles. Outside times of disagreement between the two MAX-DOAS instruments, shown in gray on Fig. 6, the correlation observed between the DOAS data and CIMS data is $R = 0.70$, which is similar to correlation of MAX-DOAS and long path DOAS measurements observed by Frieß et al. (2011). The CIMS and LP-DOAS were previously shown to agree well, particularly during times of moderate wind speeds (3–8 $\mathrm{m\,s^{-1}}$) and low NO ($< 100\,\mathrm{pmol\,mol^{-1}}$ (Liao et al., 2011).

3.5 Relationship between amount observed and vertical distribution of BrO

Figure 4 shows the timeseries of the $\mathrm{VCD_{200\,m}}$ and LT-VCD. LT-VCD values over the course of this study ranged from zero to $8 \times 10^{13}\,\mathrm{molecules\,cm^{-2}}$ with an average of $1.46 \times 10^{13}\,\mathrm{molecules\,cm^{-2}}$ and the top quartile being above $2.0 \times 10^{13}\,\mathrm{molecules\,cm^{-2}}$, which we will later consider to be "highly activated" events. LT-VCD retrieval errors had a mean of $3.9 \times 10^{12}\,\mathrm{molecules\,cm^{-2}}$ over the course of the campaign. Figure 8 shows the percentage of the LT-VCD present in the lowest 200 m ranges from shallow layer events observed primarily below 200 m to distributed column events that are also observed at higher altitudes. The third panel of Fig. 4 shows a timeseries of this ratio. Surface layer percentages over this campaign ranged between near zero and 80 %, with the highest LT-VCD observed during distributed column events with $\mathrm{VCD_{200m}}$/LT-VCD percentages of around 10 %. As the coloration of Fig. 8 indicates, high near surface mixing ratios do not always

imply high LT-VCD. In most cases, high LT-VCDs are associated with distributed column events.

3.6 Dependence on local meterology

To examine atmospheric stability, we used meteorological balloon sounding data to calculate the temperature gradient ($\mathrm{d}T/\mathrm{d}z$) near the surface. We calculated the slope of a linear fit of the first three data points of the sounding, which typically corresponds to an altude range from the surface to 200 m above ground level. Because MAX-DOAS data are daylight only, to compare our BrO measurements with the sounding data, we used daily averages of the fraction of near-surface BrO to LT-VCD from each day and examined the relationship between daily averaged ratios and the corresponding temperature gradients obtained from the local daytime sounding. Figure 9 shows the relationship between these two quantities. This box and whisker plot is generated by splitting daily observations into three bins of about 20 days each. The median is given by the red lines and shows the general trend that more stable atmospheres with inverted temperature structures (right bin) have more BrO present in the surface layer, while unstable atmospheres (left bin) tend to have BrO more distributed throughout the lower troposphere. Given that the temperature gradient likely varies at a higher rate than captured by daily sounding data, there is likely to be a smoothing effect that worsens the relationship between BrO vertical distribution and local stability. However, a clear relationship is still observed in Fig. 9.

The left panel of Fig. 10 illustrates the relationship between surface temperature and the amount of BrO in the near surface layer. On average, there is a higher fraction of BrO in the near surface layer when temperatures are below $-25\,^{\circ}\mathrm{C}$, with more distributed column BrO events being observed at higher temperatures. Figure 10 (right panel) shows that activation events in excess of $2 \times 10^{13}\,\mathrm{molecules\,cm^{-2}}$ occur at various temperatures.

Additionally, we examine the response of both the total activation as measured by the LT-VCD and the vertical distribution of BrO to wind speed. Figure 11 (left panel) shows LT-VCD values in excess of $2 \times 10^{13}\,\mathrm{molecules\,cm^{-2}}$ at various wind speeds and, as shown by the red line, there is no obvious relationship between the LT-VCD and wind speed. The

observed lack of dependence of the LT-VCD on wind speed and temperature is consistent with the observations of Halfacre et al. (2014). However, the vertical distributon of BrO is influenced by windspeed. The right panel of Fig. 11 shows the majority of shallow layer events occur during times when wind speeds are between 3–6 $\mathrm{m\,s^{-1}}$. Additionally, events at wind speeds in excess of 8 $\mathrm{m\,s^{-1}}$ tend to be more distributed throughout the column.

4 Discussion

4.1 Role of atmospheric stability

The third panel of Fig. 4 shows the vertical structure of BrO was highly variable over the course of this study. Events range from shallow layer events where most of the observed BrO is found in the lowest 200 m to distributed column events with BrO present throughout the lower troposphere. Figure 8 shows the highest observed LT-VCDs were observed during distributed column events while shallow layer events, despite their enhanced near surface mixing ratios, did not result in large amounts of total activation, as measured by the LT-VCD. This finding points out the difficulty in comparing satellite BrO column retrievals with surface observations (e.g. Sihler et al., 2012). Figure 9 shows the vertical distribution of BrO is clearly influenced by the observed atmospheric stability. During times of inversion, bromine activation events tend toward the shallow layer end of the spectrum. When the atmosphere is less stable, events tend to be distributed throughout the column. Given that this study only uses daily sounding data, and knowing that convective mixing has a strong diurnal variability, it is likely this study represents a lower bound on the influence of atmospheric stability.

Ozone depletion events have been shown to be highly variable in vertical extent (e.g. Bottenheim et al., 2002b; Tarasick and Bottenheim, 2002; Jones et al., 2010; Oltmans et al., 2012; Helmig et al., 2012). More recently, Moore et al. (2014) observed that opening of leads enhanced vertical mixing leading to a recovery of ozone and gaseous elemental mercury in the near surface layer. This mixing potentially impacts the vertical distribution of

halogens as well. McElroy et al. (1999) observed high total tropospheric BrO events and interpreted them as arising from convective vertical mixing associated with open leads that brought near-surface BrO to the free troposphere. Therefore, it is reasonable that vertical mixing or hindered mixing due to atmospheric stability affects the vertical structure of BrO.

Seasonal and temperature trends are consistent with atmospheric stability's influence on the BrO vertical structure. Figure 10 shows that at lower temperatures, which are more prevalent early in the season, events tend to be observed in shallow layers and transition to more vertically distributed as the surface temperature increases. These observations are consistent with the idea that the distribution of BrO is primarily influenced by atmospheric stability.

The right panel of Fig. 10 indicates that significant activation events happen at a variety of temperatures. Pöhler et al. (2010) observed there was a linear trend of decreasing near surface maximum BrO, observed with LP-DOAS, as temperature increased up to $-15\,^{\circ}\mathrm{C}$. When examining the whole LT-VCD, rather than a near surface concentration, this trend does not appear, however, Fig. 10 (left panel) shows a distinct preference toward near surface distributions of BrO at lower temperatures, which as Fig. 8 shows, often contain higher near surface amounts of BrO, but have a lower overall LT-VCD. The observation of Pöhler et al. (2010) of decreasing surface BrO mixing ratio at higher temperatures could therefore reflect increased vertical mixing of surface-sourced BrO that dilutes the surface concentration upon warming rather than being indicative of decreased halogen activation chemistry at higher temperatures. Figure 12 illustrates the diurnal behavior of both the LT-VCD, shown in blue, and the $\mathrm{VCD}_{200\,\mathrm{m}}$ shown in red. Boylan et al. (2014) observed diurnal boundary layer growth at Barrow in 2009, although this was less prounced during times of strong inversion. The $\mathrm{VCD}_{200\,\mathrm{m}}$ observed in Fig. 12 is similar to surface concentration data observed by Pöhler et al. (2010) as well as Stutz et al. (2011). Stutz et al. (2011) suggest this pattern is indicative of snow-sourced reactive bromine diluting through a growing boundary layer. The link between atmospheric stability and the vertical distribution of BrO demonstrated in this work supports the idea that the diurnal cycling observed is due to dilution of snow-sourced reactive bromine. The MAX-DOAS observations of the present study also allow observa-

tion of the BrO LT-VCD, which Fig. 12 shows increases to a peak in the late afternoon, which is not fully explained by dilution of a surface source because dilution would leave the LT-VCD unchanged. This growth in LT-VCD with increased mixing was also observed in the modeling work of Toyota et al. (2014). Potential explanations for this observed growth in the LT-VCD include an enhancement of reactive bromine production in the snowpack due to increased sunlight, enhanced activation of bromine occurring aloft, potentially due to heterogeneous recycling on aerosol particles, or an increased BrO lifetime aloft.

4.2 Role of wind speed

Figure 11 (left panel) shows that activation events with BrO LT-VCDs in the top quartile occur across a spectrum of wind speeds, rather than at just the low surface wind speeds associated with stable boundary layers, or high wind speeds associated with blowing snow events. The right panel of Fig. 11 shows a peak in shallow layer events between 3–6 $m\,s^{-1}$ suggesting that some ventilation of the snowpack, which has been shown to be an effective source of Br_2 (Pratt et al., 2013), is required for the release of BrO during shallow layer events. For the most part, observed wind speeds exceeding 8 $m\,s^{-1}$, led to vertically distributed events, but beyond that there is little evidence to support the need for high winds or blowing snow to sustain halogen activation aloft, consistent with the conclusions of Halfacre et al. (2014). This finding suggests that, during the course of this study, high wind events and blowing snow were not required to observe significant halogen activation. Activation events in the top quartile were observed across a range of wind speeds, particularly at more moderate wind speeds, with 66 % of highly activated events occurring at wind speeds between 3 and 8 $m\,s^{-1}$. This distribution suggests that enhanced ventilation of the snowpack, and subsequent vertical mixing of snowpack-influenced airmasses, is likely responsible for the majority of elevated LT-VCDs observed over the course of this study.

Jones et al. (2009) and Yang et al. (2010) rely on satellite observations of BrO rather than ground-based measurements to draw conclusions about the role of wind in halogen activation events. The differing viewing geometry could potentially affect the interpretation of the data when clouds are present, as shallow layer events occurring below clouds would poten-

tially be masked from the satellite view, but observable with ground-based MAX-DOAS. In contrast, BrO above a cloud that would be potentially observed by a satellite would not be detected by ground-based MAX-DOAS. Sihler et al. (2012) observed that satellite measurements could underestimate the amount of BrO during shallow layer events, implying events with distributed column vertical structure are more likely to be satellite detectable. This idea that shallow layer events may not be satellite detectable is also supported by the modeling work of Toyota et al. (2014). Enhanced visibility of the larger in magnitude and more vertically distributed BrO events could potentially explain why satellite remote sensing of BrO may show a relationship to wind speed. These differences should be considered when trying to resolve differences between ground-based and satellite-based measurements.

4.3 Relationship between activation and aerosol particles

The near-surface aerosol particle extinction retrieved from our MAX-DOAS measurements is a proxy for suspended particulate surface area that enhances recycling of halogens, allowing us to examine the relationship between BrO and aerosol particles. The left panel of Fig. 13 shows an increase in the $VCD_{200\,m}$ with increased aerosol particle extinction, while the right panel shows that the relationship between aerosol particles and the LT-VCD is less clear. Laboratory studies (e.g. Huff and Abbatt, 2000; Wren et al., 2013) and field studies (e.g. Pratt et al., 2013) indicate that pH is an important control on heterogeneous recycling of halogens. Although we are unable to determine the pH of these particles by MAX-DOAS, we simply point out that, not only is the presence of suspended surface area important, but also that the chemical composition of that surface is likely a controlling factor.

Prior to using these data to consider the role of blowing snow in observed halogen activation during this study, it is important to point out that the lack of LT-VCD observations at high aerosol optical depth, shown in Fig. 3, could potentially lead to preferential exclusion of blowing snow events from further analysis of the total amount of activation as measured by the LT-VCD. To examine the potential impacts of data exclusions, we examined the amount of data at high wind speeds discarded by the application of methods described in Sect. 2.4. Of the 147 measurements occurring when wind speeds exceeded $8\,m\,s^{-1}$ threshold used

for blowing snow in Jones et al. (2009), 86 of those were rejected due to insufficient information content. If one were to presume these were all blowing snow events and belonged in the top quartile of observed activation events, they would represent 9.6 % of LT-VCD observations and 29 % of events where the LT-VCD exceeded 2×10^{13} molecules cm^{-2}. Therefore, we find that the exclusion of low visibility data at high wind speed could only explain a small fraction of halogen activation events. While we end up discarding a significant amount of data, these filtered data still provide a fair idea of the role of high wind events, blowing snow or otherwise, in halogen activation.

While the increase in $VCD_{200\,m}$ during times of high aerosol particle extinction supports blowing snow as one source of halogens, examining the dependence of the aerosol particle extinction on wind speed, shown by the coloration in the left panel of Fig. 13, shows there is no apparent increase in extinction at high wind speeds, which we would expect if blowing snow was the only source of particulate surface area for halogen recycling. The observation of aerosol particle extinction values in excess of 10^{-1} km^{-1} across a variety of wind speeds suggests that blowing snow is not the only source of the aerosol particles needed to sustain halogen activation aloft.

Additionally, it is interesting to note that LT-VCD above 2×10^{13} molecules cm^{-2} often occur at wind speeds well below typical thresholds for blowing snow (8 m s^{-1}, Jones et al., 2009), as shown in the left panel of Fig. 11. While blowing snow is not simply a univariate function of wind speed (Sturm and Stuefer, 2013), given 9 % of observations occurred when wind speeds exceeded 8 m s^{-1} and halogen activation events in excess of 2×10^{13} molecules cm^{-2} occurred 25 % of the time, immediate activation during blowing snow events is not the sole driver of halogen activation over the course of this study, and likely some other aerosol particle source is required. Frieß et al. (2011) postulated that aerosol particles produced by sublimation of blowing snow could transport and increase observed aerosol particle extinction while also providing a suspended surface for the recycling of halogens aloft. Further, in the Arctic springtime, Hara et al. (2002) observed bromide loss from coarse sea salt particles and addition to fine sulfate particles, supporting the suggestion of bromine recycling on aerosol particles.

5 Conclusions

The methods described in this paper outline the reduction of vertical profiles retrieved from MAX-DOAS observations using optimal estimation to produce two quantities, the lower tropospheric vertical column density (LT-VCD), and the near surface vertical column density in the lowest 200 m ($VCD_{200\,m}$) that appropriately reflect the information content of ground-based MAX-DOAS measurements for timeseries analysis. Consideration of BrO averaging kernels and degrees of freedom resulting from optimal estimation validates that these quantities are most appropriate to express the two degrees of freedom observed. This method allows for identification of time periods when MAX-DOAS measurements contain information about BrO beyond the near surface layer, and evaluate how the vertical structure of BrO responds to various environmental factors. Application of these methods shows retrieval of LT-VCDs by ground-based MAX-DOAS is highly dependent on visibility. During this study, we retrieved the LT-VCD 50 % of the time.

The vertical structure of BrO is highly variable, with the fraction of lower-tropospheric BrO in the lowest 200 m varying from near zero to nearly 80 %. The vertical distribution of activation events is clearly influenced by the atmospheric stability. This influence also manifests itself when examining the influence of temperature and seasonality. Later in the season, higher temperatures, and likely enhanced vertical mixing, tend to result in more BrO aloft than early in the season, where activation takes place in shallower layers. LT-VCD values in excess of 2×10^{13} molecules cm^{-2} occur across a variety of temperatures and wind speeds, but they are typically associated with distributed column events, rather than shallow layer events. Events that have larger observed near surface mixing ratios are typically of the shallow layer variety and do not typically have large amounts of BrO spread through the lower troposphere, potentially implying less overall ozone depletion and deposition of mercury from these events. This implies that both surface and upper profile measurements are necessary to appropriately identify the impact of environmental variables on O_3 depletion and Hg oxidation rates and extent.

The observed BrO $VCD_{200\,m}$ showed diurnal cycling, suggesting a surface snow source of reactive bromine diluting through an expanded boundary layer, which reflects the link between atmospheric stability and the vertical distribution of BrO. The observed growth in the LT-VCD during the day indicates the production, or lifetime of reactive bromine is not static, but production increases throughout the day, or losses decrease. The BrO $VCD_{200\,m}$ also showed an increase during times of high aerosol particle extinction, however the lack of a clear relationship between aerosol particle extinction and wind speed implies that blowing snow is not the sole source of aerosol particles needed for heterogeneous recycling of bromine aloft.

High wind events were not common over the course of this study. While high winds did lead to some of the highest measured columns of BrO, given the low frequency of these events, high wind events, blowing snow or otherwise, are not the sole driver of halogen activation over the course of this study, suggesting that mechanisms requiring only moderate wind speeds (e.g. wind pumping) are important for halogen activation in the Arctic.

The Supplement related to this article is available online at doi:10.5194/acpd-0-1-2015-supplement.

Acknowledgements. The research at the University of Alaska was supported by the National Aeronautics and Space Administration (NASA) Cryospheric Sciences Program (CSP), and partial financial support for MAX-DOAS analysis methods was provided by the National Science Foundation under grant ARC-1023118. The Purdue group recognizes NSF support through grant ARC-1107695. K. A. Pratt was supported by a NSF Postdoctoral Fellowship in Polar Regions Research. The Purdue group acknowledges field assistance from Kyle Custard (Purdue Univ.), David Tanner (Georgia Tech), and L. Gregory Huey (Georgia Tech). The research at the Jet Propulsion Laboratory, California Institute of Technology, was supported by the NASA CSP. The authors gratefully acknowledge Chris Moore (Desert Research Inst.) for helpful discussions, as well as Alexei Rozanov from IUP Bremen for providing the SCIATRAN radiative transfer code. The authors also wish to thank UMIAQ for logistical support, and Bristow Air for providing a helicopter for the deployment of IL1.

References

Abbatt, J. P. D., Thomas, J. L., Abrahamsson, K., Boxe, C., Granfors, A., Jones, A. E., King, M. D., Saiz-Lopez, A., Shepson, P. B., Sodeau, J., Toohey, D. W., Toubin, C., von Glasow, R., Wren, S. N., and Yang, X.: Halogen activation via interactions with environmental ice and snow in the polar lower troposphere and other regions, Atmos. Chem. Phys., 12, 6237–6271, doi:10.5194/acp-12-6237-2012, 2012.

Barrie, L. A., Bottenheim, J. W., Schnell, R. C., Crutzen, P. J., and Rasmussen, R. A.: Ozone destruction and photochemical reactions at polar sunrise in the lower Arctic atmosphere, Nature, 334, 138–141, doi:10.1038/334138a0, 1988.

Bottenheim, J. W., Fuentes, J. D., Tarasick, D. W., and Anlauf, K. G.: Ozone in the Arctic lower troposphere during winter and spring 2000 (ALERT2000), Atmos. Environ., 36, 2535–2544, doi:10.1016/S1352-2310(02)00121-8, 2002.

Boylan, P., Helmig, D., Staebler, R., Turnipseed, A., Fairall, C., and Neff, W.: Boundary layer dynamics during the Ocean-Atmosphere-Sea-Ice-Snow (OASIS) 2009 experiment at Barrow, AK, Journal of Geophysical Research: Atmospheres, 119, 2261–2278, doi:10.1002/2013JD020299, 2014.

Carlson, D., Donohoue, D., Platt, U., and Simpson, W. R.: A low power automated MAX-DOAS instrument for the Arctic and other remote unmanned locations, Atmos. Meas. Tech., 3, 429–439, doi:10.5194/amt-3-429-2010, 2010.

Chance, K.: Analysis of BrO measurements from the global ozone monitoring experiment, Geophys. Res. Lett., 25, 3335–3338, 1998.

Chance, K. V. and Spurr, R. J.: Ring effect studies: Rayleigh scattering, including molecular parameters for rotational Raman scattering, and the Fraunhofer spectrum, Appl. Optics, 36, 5224–5230, 1997.

Deutschmann, T., Beirle, S., Frieß, U., Grzegorski, M., Kern, C., Kritten, L., Platt, U., Prados-Román, C., Puķıte, J., Wagner, T., Werner, B., and Pfeilsticker, K.: The Monte Carlo atmospheric radiative transfer model McArtim: Introduction and validation of Jacobians and 3D features, J. Quant. Spectrosc. Ra., 112, 1119–1137, doi:10.1016/j.jqsrt.2010.12.009, 2011.

Fan, S.-M., and Jacob, D. J.: Surface ozone depletion in Arctic spring sustained by bromine reactions on aerosols, Nature, 359, 522–524, doi:10.1038/359522a0, 1992.

Fayt, C., De Smedt, I., Letocart, V., Merlaud, A., Pinardi, G., Van Roozendael, M., and Roozendael, M. V. A. N.: QDOAS Software User Manual, available at: http://uv-vis.aeronomie.be/software/QDOAS/index.php (last access: 10 March 2014), 2011.

Fickert, S., Adams, J. W., and Crowley, J. N.: Activation of Br_2 and BrCl via uptake of HOBr onto aqueous salt solutions, J. Geophys. Res., 104, 23719–23727, doi:10.1029/1999JD900359, 1999.

Foster, K. L., Plastridge, R. A., Bottenheim, J. W., Shepson, P. B., Finlayson-Pitts, B. J., and Spicer, C. W.: The role of Br_2 and BrCl in surface ozone destruction at polar sunrise, Science, 291, 471–474, 2001.

Frieß, U.: Dynamics and chemistry of tropospheric bromine explosion events in the Antarctic coastal region, Journal of Geophysical Research, 109, D06 305, doi:10.1029/2003JD004133, 2004.

Frieß U., Monks, P. S., Remedios, J. J., Rozanov, A., Sinreich, R., Wagner, T., and Platt, U.: MAX-DOAS O_4 measurements: a new technique to derive information on atmospheric aerosols: 2. Modeling studies, J. Geophys. Res., 111, D14203, doi:10.1029/2005JD006618, 2006.

Frieß U., Sihler, H., Sander, R., Pöhler, D., Yilmaz, S., and Platt, U.: The vertical distribution of BrO and aerosols in the Arctic: measurements by active and passive differential optical absorption spectroscopy, J. Geophys. Res., 116, D00R04, doi:10.1029/2011JD015938, 2011.

Halfacre, J. W., Knepp, T. N., Shepson, P. B., Thompson, C. R., Pratt, K. A., Li, B., Peterson, P. K., Walsh, S. J., Simpson, W. R., Matrai, P. A., Bottenheim, J. W., Netcheva, S., Perovich, D. K., and Richter, A.: Temporal and spatial characteristics of ozone depletion events from measurements in the Arctic, Atmos. Chem. Phys., 14, 4875–4894, doi:10.5194/acp-14-4875-2014, 2014.

Hara, K., Osada, K., Matsunaga, K., Iwasaka, Y., Shibata, T., and Furuya, K.: Atmospheric inorganic chlorine and bromine species in Arctic boundary layer of the winter/spring, J. Geophys. Res., 107, 4361, doi:10.1029/2001JD001008, 2002.

Helmig, D., Boylan, P., Johnson, B., Oltmans, S., Fairall, C., Staebler, R., Weinheimer, A., Orlando, J., Knapp, D. J., Montzka, D. D., Flocke, F., Frieß, U., Sihler, H., and Shepson, P. B.: Ozone dynamics and snow-atmosphere exchanges during ozone depletion events at Barrow, Alaska, J. Geophys. Res.-Atmos., 117, D20303, doi:10.1029/2012JD017531, 2012.

Hermans, C., Vandaele, A., Coquart, B., Jenouvrier, A., Merienne, M. F., Fally, S., Carleer, M., and Colin, R.: Absorption bands of O_2 and its collision-induced bands in the 30 000–7500 cm^{-1} wavenumber region, in: IRS 2000: Current Problems in Atmospheric Radiation, edited by: Smith, W. L. and Timofeyev, Y. M., Hampton, VA, Deepak, 639–642, 2001.

Hönninger, G., von Friedeburg, C., and Platt, U.: Multi axis differential optical absorption spectroscopy (MAX-DOAS), Atmos. Chem. Phys., 4, 231–254, doi:10.5194/acp-4-231-2004, 2004.

Huff, A. K. and Abbatt, J. P. D.: Gas-phase Br_2 production in heterogeneous reactions of Cl_2, HOCl, and BrCl with halide-ice surfaces, J. Phys. Chem. A, 104, 7284–7293, doi:10.1021/jp001155w, 2000.

Jones, A. E., Anderson, P. S., Begoin, M., Brough, N., Hutterli, M. A., Marshall, G. J., Richter, A., Roscoe, H. K., and Wolff, E. W.: BrO, blizzards, and drivers of polar tropospheric ozone depletion events, Atmos. Chem. Phys., 9, 4639–4652, doi:10.5194/acp-9-4639-2009, 2009.

Jones, A. E., Anderson, P. S., Wolff, E. W., Roscoe, H. K., Marshall, G. J., Richter, A., Brough, N., and Colwell, S. R.: Vertical structure of Antarctic tropospheric ozone depletion events: characteristics and broader implications, Atmos. Chem. Phys., 10, 7775–7794, doi:10.5194/acp-10-7775-2010, 2010.

Koo, J.-H., Wang, Y., Kurosu, T. P., Chance, K., Rozanov, A., Richter, A., Oltmans, S. J., Thompson, A. M., Hair, J. W., Fenn, M. A., Weinheimer, A. J., Ryerson, T. B., Solberg, S., Huey, L. G., Liao, J., Dibb, J. E., Neuman, J. A., Nowak, J. B., Pierce, R. B., Natarajan, M., and Al-Saadi, J.: Characteristics of tropospheric ozone depletion events in the Arctic spring: analysis of the ARCTAS, ARCPAC, and ARCIONS measurements and satellite BrO observations, Atmos. Chem. Phys., 12, 9909–9922, doi:10.5194/acp-12-9909-2012, 2012.

Krnavek, L., Simpson, W. R., Carlson, D., Domine, F., Douglas, T. A., and Sturm, M.: The chemical composition of surface snow in the Arctic: examining marine, terrestrial, and atmospheric influences, Atmos. Environ., 50, 349–359, doi:10.1016/j.atmosenv.2011.11.033, 2012.

Lehrer, E., Hönninger, G., and Platt, U.: A one dimensional model study of the mechanism of halogen liberation and vertical transport in the polar troposphere, Atmos. Chem. Phys., 4, 2427–2440, doi:10.5194/acp-4-2427-2004, 2004.

Liao, J., Sihler, H., Huey, L. G., Neuman, J. A., Tanner, D. J., Friess, U., Platt, U., Flocke, F. M., Orlando, J. J., Shepson, P. B., Beine, H. J., Weinheimer, A. J., Sjostedt, S. J., Nowak, J. B., Knapp, D. J., Staebler, R. M., Zheng, W., Sander, R., Hall, S. R., and Ullmann, K.: A comparison of Arctic BrO measurements by chemical ionization mass spectrometry and long path-differential optical absorption spectroscopy, J. Geophys. Res., 116, 1–14, doi:10.1029/2010JD014788, 2011.

Liao, J., Huey, L. G., Tanner, D. J., Flocke, F. M., Orlando, J. J., Neuman, J. A., Nowak, J. B., Weinheimer, A. J., Hall, S. R., Smith, J. N., Fried, A., Staebler, R. M., Wang, Y., Koo, J.-H., Cantrell, C. A., Weibring, P., Walega, J., Knapp, D. J., Shepson, P. B., and Stephens, C. R.: Observations of inorganic bromine (HOBr, BrO, and Br_2) speciation at Barrow, Alaska, in spring 2009, J. Geophys. Res., 117, D00R16, doi:10.1029/2011JD016641, 2012.

Liao, J., Huey, L. G., Liu, Z., Tanner, D. J., Cantrell, C. A., Orlando, J. J., Flocke, F. M., Shepson, P. B., Weinheimer, A. J., Hall, S. R., Ullmann, K., Beine, H. J., Wang, Y., Ingall, E. D., Stephens, C. R., Hornbrook, R. S., Apel, E. C., Riemer, D., Fried, A., Mauldin III, R. L., Smith, J. N., Staebler, R. M., Neuman, J. A., and Nowak, J. B.: High levels of molecular chlorine in the Arctic atmosphere, Nat. Geosci., 7, 91–94, doi:10.1038/ngeo2046, 2014.

Malicet, J., Daumont, D., Charbonnier, J., Parisse, C., Chakir, A., and Brion, J.: Ozone UV spectroscopy. II. Absorption cross-sections and temperature dependence, J. Atmos. Chem., 21, 263–273, doi:10.1007/BF00696758, 1995.

McConnell, J. C., Henderson, G. S., Barrie, L., Bottenheim, J., Niki, H., Langford, C. H., and Templeton, E. M. J.: Photochemical bromine production implicated in Arctic boundary-layer ozone depletion, Nature, 355, 150–152, doi:10.1038/355150a0, 1992.

McElroy, C. T., McLinden, C. A., and McConnell, J. C.: Evidence for bromine monoxide in the free troposphere during the arctic polar sunrise, Nature, 397, 338–341, 1999.

Moore, C. W., Obrist, D., Steffen, A., Staebler, R. M., Douglas, T. A., Richter, A., and Nghiem, S. V.: Convective forcing of mercury and ozone in the Arctic boundary layer induced by leads in sea ice., Nature, 506, 81–84, doi:10.1038/nature12924, 2014.

Mozurkewich, M.: Mechanisms for the release of halogens from sea-salt particles by free radical reactions, J. Geophys. Res., 100, 14199–14207, 1995.

Neuman, J. A., Nowak, J. B., Huey, L. G., Burkholder, J. B., Dibb, J. E., Holloway, J. S., Liao, J., Peischl, J., Roberts, J. M., Ryerson, T. B., Scheuer, E., Stark, H., Stickel, R. E., Tanner, D. J., and Weinheimer, A.: Bromine measurements in ozone depleted air over the Arctic Ocean, Atmos. Chem. Phys., 10, 6503–6514, doi:10.5194/acp-10-6503-2010, 2010.

Nghiem, S. V., Clemente-Colón, P., Douglas, T., Moore, C., Obrist, D., Perovich, D. K., Pratt, K. A., Rigor, I. G., Simpson, W., Shepson, P. B., Steffen, A., and Woods, J.: Studying bromine, ozone, and mercury chemistry in the Arctic, EOS T. Am. Geophys. Un., 94, 289–291, doi:10.1002/2013EO330002, 2013.

Oltmans, S. J., Johnson, B. J., and Harris, J. M.: Springtime boundary layer ozone depletion at Barrow, Alaska: meteorological influence, year-to-year variation, and long-term change, J. Geophys. Res., 117, D00R18, doi:10.1029/2011JD016889, 2012.

Parrella, J. P., Jacob, D. J., Liang, Q., Zhang, Y., Mickley, L. J., Miller, B., Evans, M. J., Yang, X., Pyle, J. A., Theys, N., and Van Roozendael, M.: Tropospheric bromine chemistry: implications for present and pre-industrial ozone and mercury, Atmos. Chem. Phys., 12, 6723–6740, doi:10.5194/acp-12-6723-2012, 2012.

Payne, V. H., Clough, S. A., Shephard, M. W., Nassar, R., and Logan, J. A.: Information-centered representation of retrievals with limited degrees of freedom for signal: application to methane from the tropospheric emission spectrometer, J. Geophys. Res., 114, D10307, doi:10.1029/2008JD010155, 2009.

Piot, M. and von Glasow, R.: The potential importance of frost flowers, recycling on snow, and open leads for ozone depletion events, Atmos. Chem. Phys., 8, 2437–2467, doi:10.5194/acp-8-2437-2008, 2008.

Platt, U., and Hönninger, G.: The role of halogen species in the troposphere, Chemosphere, 52, 325–338, doi:10.1016/S0045-6535(03)00216-9, 2003.

Pöhler, D., Vogel, L., Friess, U., and Platt, U.: Observation of halogen species in the Amundsen Gulf, Arctic, by active long-path differential optical absorption spectroscopy, P. Natl. Acad. Sci. USA, 107, 6582–6587, doi:10.1073/pnas.0912231107, 2010.

Pratt, K. A., Custard, K. D., Shepson, P. B., Douglas, T. A., Pöhler, D., General, S., Zielcke, J., Simpson, W. R., Platt, U., Tanner, D. J., Gregory Huey, L., Carlsen, M., and Stirm, B. H.: Photochemical production of molecular bromine in Arctic surface snowpacks, Nat. Geosci., 6, 351–356, doi:10.1038/ngeo1779, 2013.

Richter, A., Wittrock, F., Eisinger, M., and Burrows, J. P.: GOME observations of tropospheric BrO in Northern Hemispheric spring and summer 1997, Geophys. Res. Lett., 25, 2683–2686, 1998.

Rodgers, C. D.: Inverse Methods For Atmospheric Sounding: Theory and Practice, World Scientific, Singapore, 2000.

Rozanov, A., Bovensmann, H., Bracher, A., Hrechanyy, S., Rozanov, V., Sinnhuber, M., Stroh, F., and Burrows, J.: NO_2 and BrO vertical profile retrieval from SCIAMACHY limb measurements: sensitivity studies, Adv. Space Res., 36, 846–854, doi:10.1016/j.asr.2005.03.013, 2005.

Saiz-Lopez, A. and von Glasow, R.: Reactive halogen chemistry in the troposphere, Chem. Soc. Rev., 41, 6448–6472, 2012.

Salawitch, R. J., Canty, T., Kurosu, T., Chance, K., Liang, Q., da Silva, A., Pawson, S., Nielsen, J. E., Rodriguez, J. M., Bhartia, P. K., Liu, X., Huey, L. G., Liao, J., Stickel, R. E., Tanner, D. J., Dibb, J. E., Simpson, W. R., Donohoue, D., Weinheimer, A., Flocke, F., Knapp, D., Montzka, D., Neuman, J. A., Nowak, J. B., Ryerson, T. B., Oltmans, S., Blake, D. R., Atlas, E. L., Kinnison, D. E., Tilmes, S., Pan, L. L., Hendrick, F., Van Roozendael, M., Kreher, K., Johnston, P. V., Gao, R. S., Johnson, B., Bui, T. P., Chen, G., Pierce, R. B., Crawford, J. H., and Jacob, D. J.: A new interpretation of total column BrO during Arctic spring, Geophys. Res. Lett., 37, L21805, doi:10.1029/2010GL043798, 2010.

Schroeder, W., Anlauf, K., Barrie, L., and Lu, J.: Arctic springtime depletion of mercury, Nature, 16–17, 394, doi:10.1038/28530, 1998.

Sihler, H., Platt, U., Beirle, S., Marbach, T., Kühl, S., Dörner, S., Verschaeve, J., Frieß, U., Pöhler, D., Vogel, L., Sander, R., and Wagner, T.: Tropospheric BrO column densities in the Arctic derived from satellite: retrieval and comparison to ground-based measurements, Atmos. Meas. Tech., 5, 2779–2807, doi:10.5194/amt-5-2779-2012, 2012.

Simpson, W. R., Carlson, D., Hönninger, G., Douglas, T. A., Sturm, M., Perovich, D., and Platt, U.: First-year sea-ice contact predicts bromine monoxide (BrO) levels at Barrow, Alaska better than potential frost flower contact, Atmos. Chem. Phys., 7, 621–627, doi:10.5194/acp-7-621-2007, 2007a.

Simpson, W. R., von Glasow, R., Riedel, K., Anderson, P., Ariya, P., Bottenheim, J., Burrows, J., Carpenter, L. J., Frieß, U., Goodsite, M. E., Heard, D., Hutterli, M., Jacobi, H.-W., Kaleschke, L., Neff, B., Plane, J., Platt, U., Richter, A., Roscoe, H., Sander, R., Shepson, P., Sodeau, J., Steffen, A., Wagner, T., and Wolff, E.: Halogens and their role in polar boundary-layer ozone depletion, Atmos. Chem. Phys., 7, 4375–4418, doi:10.5194/acp-7-4375-2007, 2007b.

Spicer, C. W., Plastridge, R. A., Foster, K. L., Finlayson-Pitts, B. J., Bottenheim, J. W., Grannas, A. M., and Shepson, P. B.: Molecular halogens before and during ozone depletion events in the Arctic at polar sunrise: concentrations and sources, Atmos. Environ., 36, 2721–2731, doi:10.1016/S1352-2310(02)00125-5, 2002.

Steffen, A., Douglas, T., Amyot, M., Ariya, P., Aspmo, K., Berg, T., Bottenheim, J., Brooks, S., Cobbett, F., Dastoor, A., Dommergue, A., Ebinghaus, R., Ferrari, C., Gardfeldt, K., Goodsite, M. E., Lean, D., Poulain, A. J., Scherz, C., Skov, H., Sommar, J., and Temme, C.: A synthesis of atmospheric mercury depletion event chemistry in the atmosphere and snow, Atmos. Chem. Phys., 8, 1445–1482, doi:10.5194/acp-8-1445-2008, 2008.

Sturm, M. and Stuefer, S.: Wind-blown flux rates derived from drifts at arctic snow fences, J. Glaciol., 59, 21–34, doi:10.3189/2013JoG12J110, 2013.

Stutz, J., Thomas, J. L., Hurlock, S. C., Schneider, M., von Glasow, R., Piot, M., Gorham, K., Burkhart, J. F., Ziemba, L., Dibb, J. E., and Lefer, B. L.: Longpath DOAS observations of surface BrO at Summit, Greenland, Atmospheric Chemistry and Physics, 11, 9899–9910, doi:10.5194/acp-11-9899-2011, 2011.

Tackett, P. J., Cavender, A. E., Keil, A. D., Shepson, P. B., Bottenheim, J. W., Morin, S., Deary, J., Steffen, A., and Doerge, C.: A study of the vertical scale of halogen chemistry in the Arc-

tic troposphere during Polar Sunrise at Barrow, Alaska, J. Geophys. Res., 112, D07306, doi:10.1029/2006JD007785, 2007.

Tarasick, D. W. and Bottenheim, J. W.: Surface ozone depletion episodes in the Arctic and Antarctic from historical ozonesonde records, Atmos. Chem. Phys., 2, 197–205, doi:10.5194/acp-2-197-2002, 2002.

Theys, N., Van Roozendael, M., Errera, Q., Hendrick, F., Daerden, F., Chabrillat, S., Dorf, M., Pfeilsticker, K., Rozanov, A., Lotz, W., Burrows, J. P., Lambert, J.-C., Goutail, F., Roscoe, H. K., and De Mazière, M.: A global stratospheric bromine monoxide climatology based on the BASCOE chemical transport model, Atmos. Chem. Phys., 9, 831–848, doi:10.5194/acp-9-831-2009, 2009.

Theys, N., Van Roozendael, M., Hendrick, F., Yang, X., De Smedt, I., Richter, A., Begoin, M., Errera, Q., Johnston, P. V., Kreher, K., and De Mazière, M.: Global observations of tropospheric BrO columns using GOME-2 satellite data, Atmos. Chem. Phys., 11, 1791–1811, doi:10.5194/acp-11-1791-2011, 2011.

Toom-Sauntry, D. and Barrie, L. A.: Chemical composition of snowfall in the high Arctic: 1990–1994, Atmos. Environ., 36, 2683–2693, 2002.

Toyota, K., McConnell, J. C., Staebler, R. M., and Dastoor, A. P.: Air–snowpack exchange of bromine, ozone and mercury in the springtime Arctic simulated by the 1-D model PHANTAS – Part 1: In-snow bromine activation and its impact on ozone, Atmos. Chem. Phys., 14, 4101–4133, doi:10.5194/acp-14-4101-2014, 2014.

Tuckermann, M., R., A., Golz, C., Lorenzen-Schmidt, H., Senne, T., Stutz, J., Trost, B., Unold, W., and Platt, U.: DOAS-observation of halogen radical-catalysed arctic boundary layer ozone destruction during the ARCTOC-campaigns 1995 and 1996 in Ny-Alesund, Spitsbergen, Tellus B, 49, 533–555, doi:10.1034/j.1600-0889.49.issue5.9.x, 1997.

Vandaele, A., Hermans, C., Simon, P., Carleer, M., Colin, R., Fally, S., Mérienne, M., Jenouvrier, A., and Coquart, B.: Measurements of the NO_2 absorption cross-section from 42 000 cm^{-1} to 10 000 cm^{-1} (238–1000 nm) at 220 K and 294 K, J. Quant. Spectrosc. Ra., 59, 171–184, doi:10.1016/S0022-4073(97)00168-4, 1998.

von Clarmann, T. and Grabowski, U.: Elimination of hidden a priori information from remotely sensed profile data, Atmos. Chem. Phys., 7, 397–408, doi:10.5194/acp-7-397-2007, 2007.

Wagner, T. and Platt, U.: Satellite mapping of enhanced BrO concentrations in the troposphere, Nature, 395, 486–490, 1998.

Wilmouth, D. M., Hanisco, T. F., Donahue, N. M., and Anderson, J. G.: Fourier transform ultraviolet spectroscopy of the $A^2\Pi_{3/2} \leftarrow X^2\Pi_{3/2}$ transition of BrO, J. Phys. Chem. A, 103, 8935–8945, doi:10.1021/jp991651o, 1999.

Wren, S. N., Donaldson, D. J., and Abbatt, J. P. D.: Photochemical chlorine and bromine activation from artificial saline snow, Atmos. Chem. Phys., 13, 9789–9800, doi:10.5194/acp-13-9789-2013, 2013.

Yang, X., Pyle, J. A., Cox, R. A., Theys, N., and Van Roozendael, M.: Snow-sourced bromine and its implications for polar tropospheric ozone, Atmos. Chem. Phys., 10, 7763–7773, doi:10.5194/acp-10-7763-2010, 2010.

Table 1. Absorber cross sections used in the MAX-DOAS fitting.

Species	Cross Section
BrO (223 K)	Wilmouth et al. (1999)
O_3 (243 K)	Malicet et al. (1995)
NO_2 (220 K)	Vandaele et al. (1998)
O_4	Hermans et al. (2001)
Ring	Determined from zenith spectra using Chance and Spurr (1997)

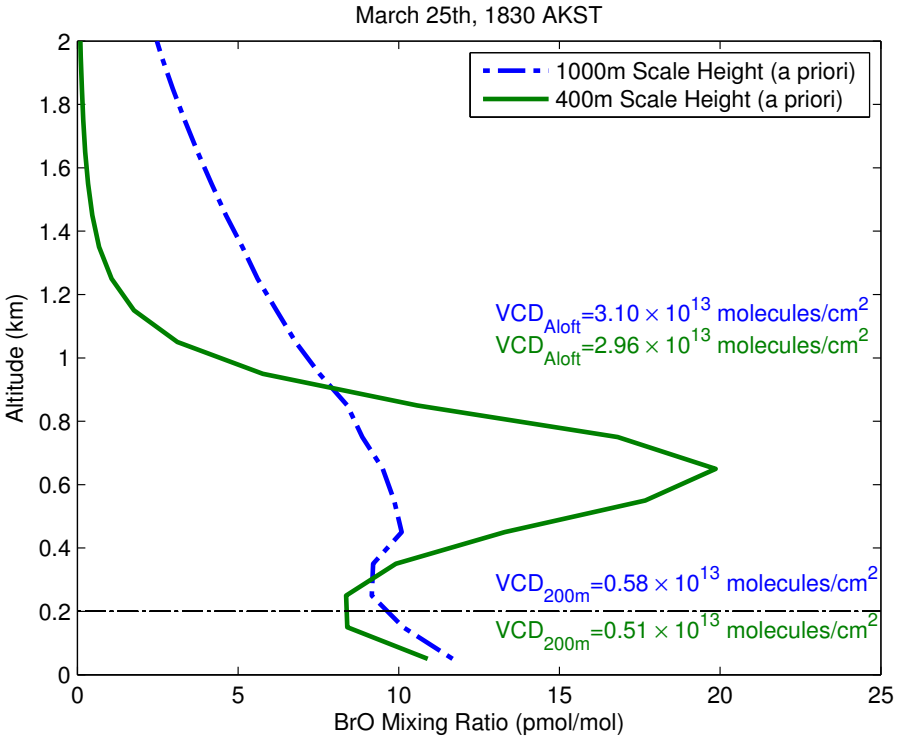

Figure 1. A sample profile retrieval of BrO at the BARC building. The blue line represents the profile retrieved using an a priori profile that exponentially decays with a scale height of 1000 m, while the green represents quantities retrieved using an a priori profile that exponentially decays with a scale height of 400 m (a priori used for this study). The dashed lines indicate layer boundaries determined from the ensemble of retrievals over the course of this study. The partial VCD values noted on the figure correspond to layer selections used in this study. The $VCD_{200\,m}$ is the integral of the retrieved profile from 0–200 m and the VCD_{Aloft} is integrated from 200 to 2000 m.

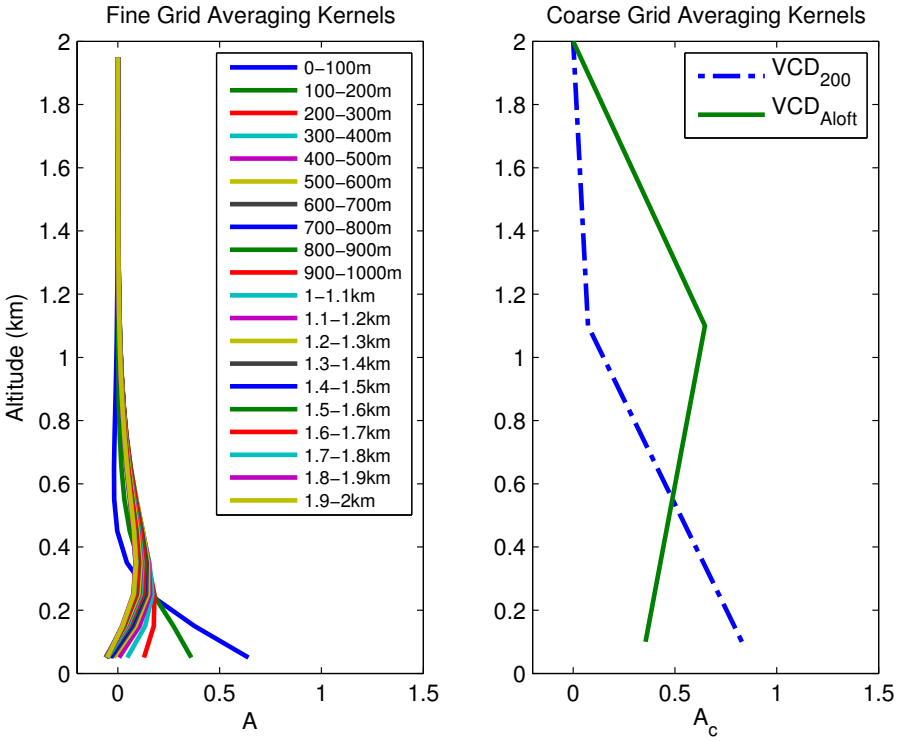

Figure 2. An illustration of the grid coarsening of the BrO averaging kernels. These averaging kernels correspond to the retrieval shown in green on Fig. 1. Averaging kernels for the original retrieval (left) and for the coarse grid (right).

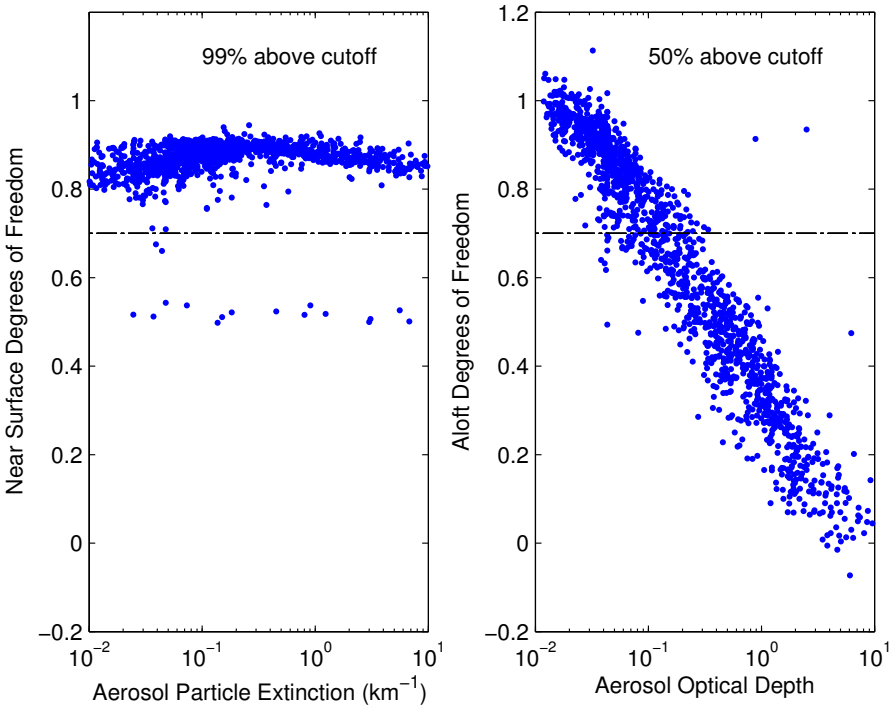

Figure 3. The left panel shows the degrees of freedom associated with the $VCD_{200\,m}$ as a function of near-surface aerosol particle extinction. The right panel shows the degrees of freedom associated with the $VCD_{Residual}$ as a function of the aerosol optical depth. The dashed line illustrates the cutoff we have chosen for sufficient information content.

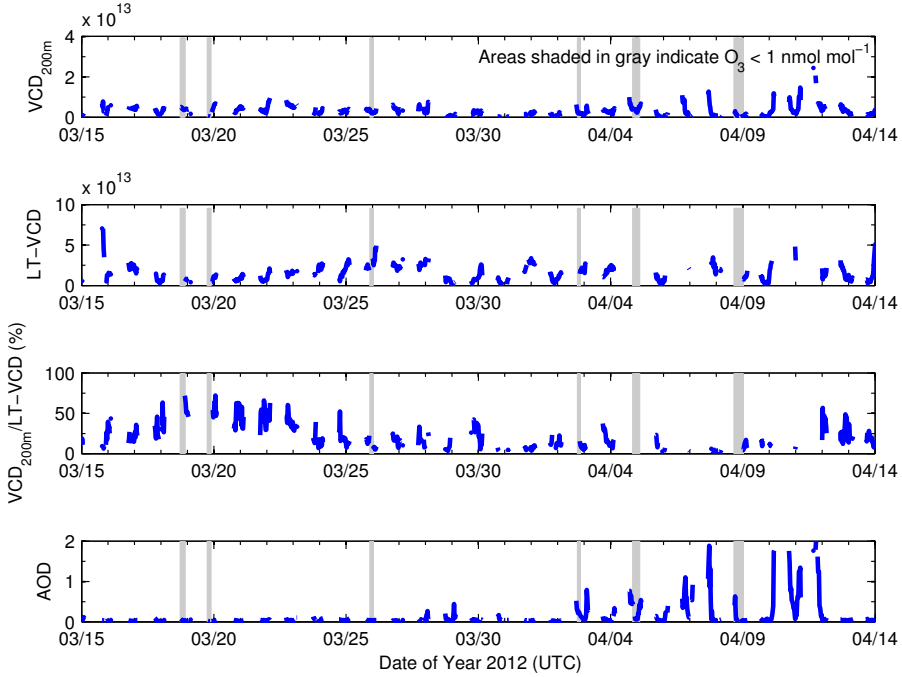

Figure 4. A portion of the timeseries of BrO observed during this study. The top panel represents the VCD_{200}, the second panel represents the LT-VCD, both of which have units of $\mathrm{molecules\,cm^{-2}}$. The third panel shows the percentage of the LT-VCD observed in the lowest 200 m, while the bottom panel shows the aerosol optical depth over the course of this study. In the third panel, ratios are not calculated for events that have a LT-VCD below $5 \times 10^{12}\,\mathrm{molecules\,cm^{-2}}$. Shaded areas represent potentially titrated air masses near the surface (Ozone $< 1\,\mathrm{nmol\,mol^{-1}}$). The full timeseries can be found in the Supplement.

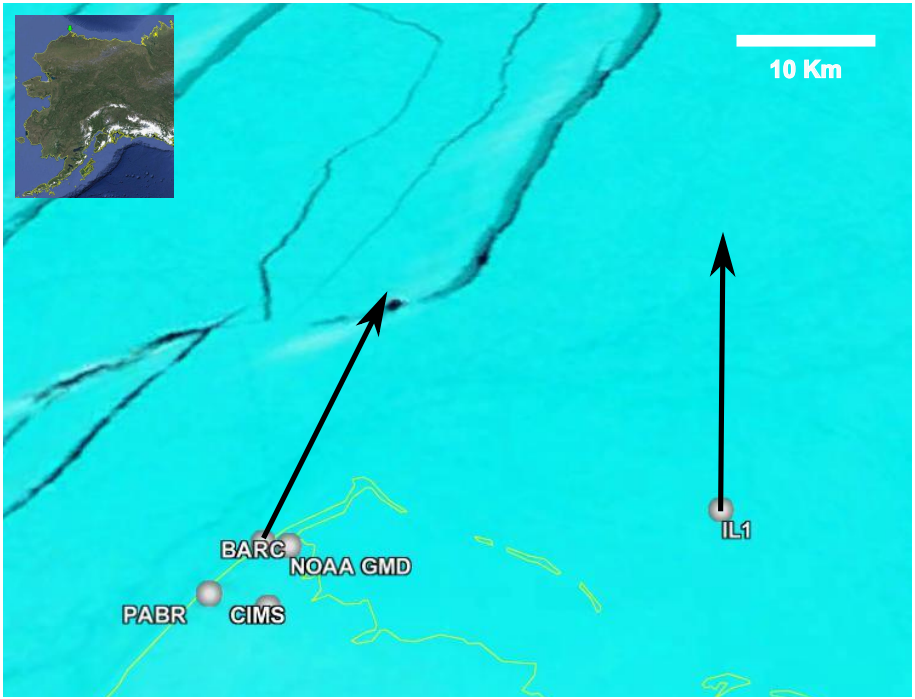

Figure 5. Field locations during the BROMEX field campaign overlain on Moderate Resolution Imaging Spectrometer data from the Aqua satellite (7,2,1 bands). This ice cover image is from March 13th, 2012. These locations are Barrow Arctic Research Center (BARC), Chemical Ionization Mass Spectrometry (CIMS), NOAA Global Monitoring Division (NOAA GMD) station, IceLander 1 (IL1) buoy, and Barrow Airport (PABR), nearby where most of Barrow's population resides. The distance between BARC and IL1 is about 36 km. Viewing azimuths for each DOAS instrument are indicated with black arrows. The inset map of Alaska shows the study location marked in green.

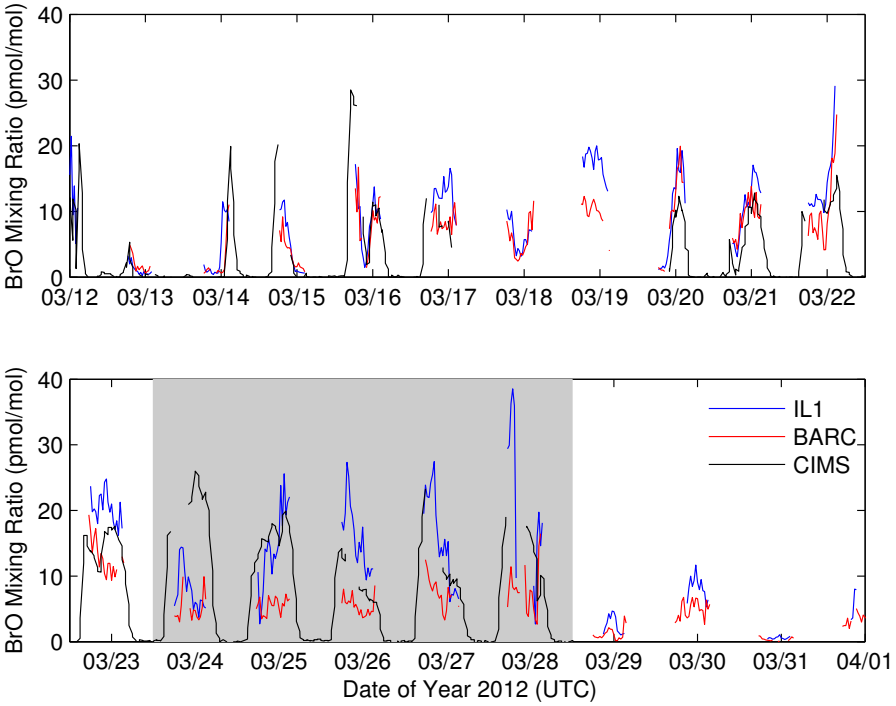

Figure 6. A timeseries of 30 min averaged BrO measured using CIMS, compared with average BrO in the lowest 100 m measured by MAX-DOAS at two different sites. The grey area indicates times when there were significant differences in BrO observed between MAX-DOAS sites at the BARC Building and on land fast ice 36 km NE of the BARC building (IL1).

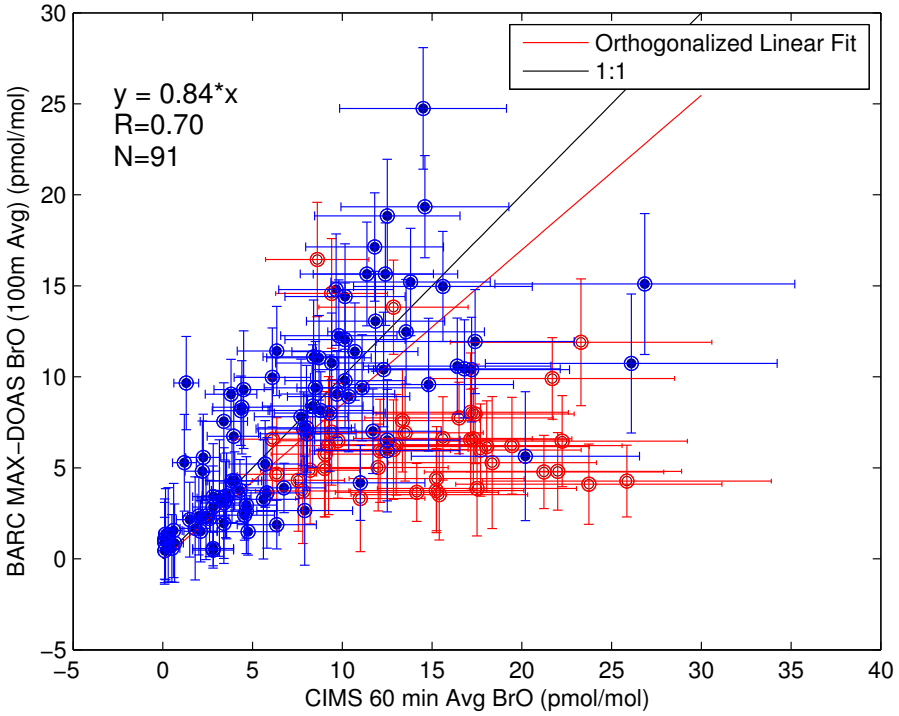

Figure 7. The correlation of 60 min averaged CIMS BrO with BrO retrieved in the lowest 100 m using MAX-DOAS. Red circles indicate times when we observed a chemical gradient between field sites, which are excluded from this correlation.

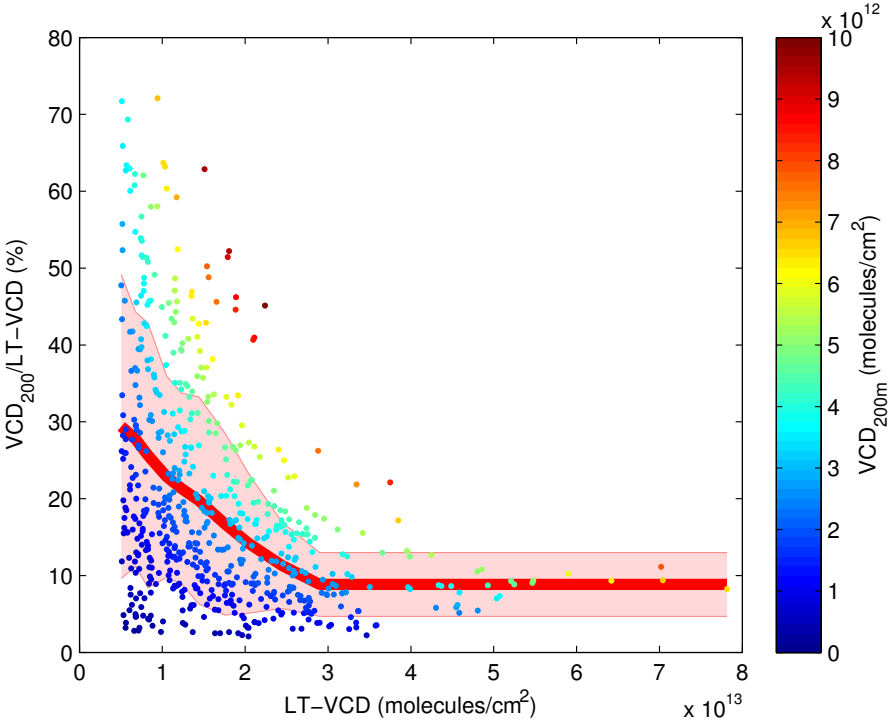

Figure 8. The relationship between the total BrO activation, as measured by the LT-VCD, and the vertical structure of the activation event. The red line represents the mean percentage of BrO in the lowest 200 m as a function of the LT-VCD, calculated from deciles on the x axis, while the shaded region represents one standard deviation. The coloration indicates the $VCD_{200\,m}$. In this plot LT-VCD values below 5×10^{12} molecules cm^{-2} are eliminated to avoid calculating percentages from near zero amounts of BrO.

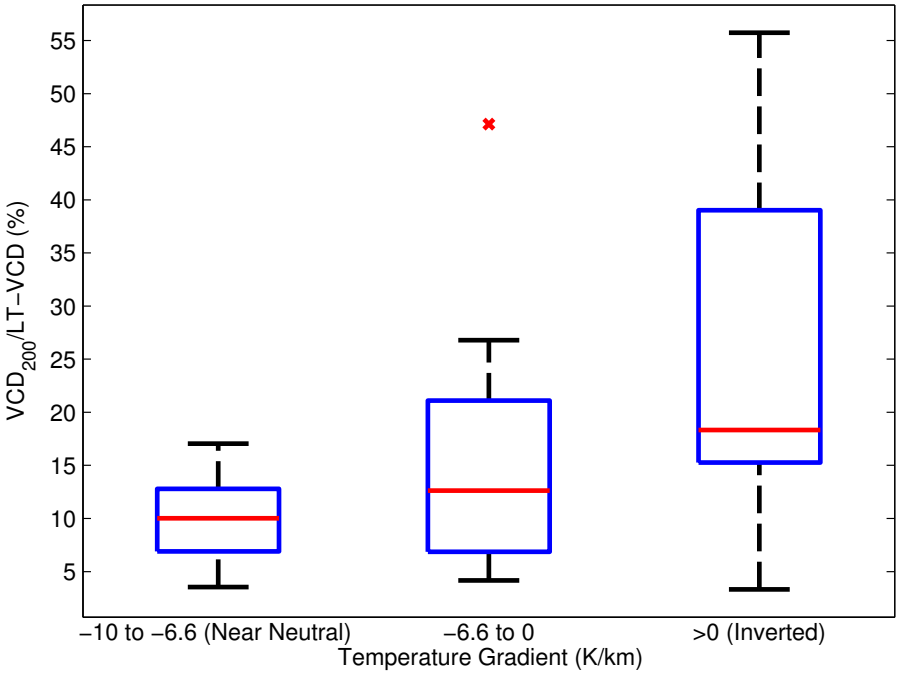

Figure 9. The relationship between daily estimated temperature gradients vs. the average percentage of BrO observed in the near surface layer during that day is shown here using a box and whisker plot. The data are split such that each bin comprises ≈ 20 days worth of data. The red lines show the median value for each bin, while the blue box encloses the 25–75th percentile and the whiskers show the full range of data excluding outliers ($\times$). Outliers are points that are outside 3σ for the corresponding group.

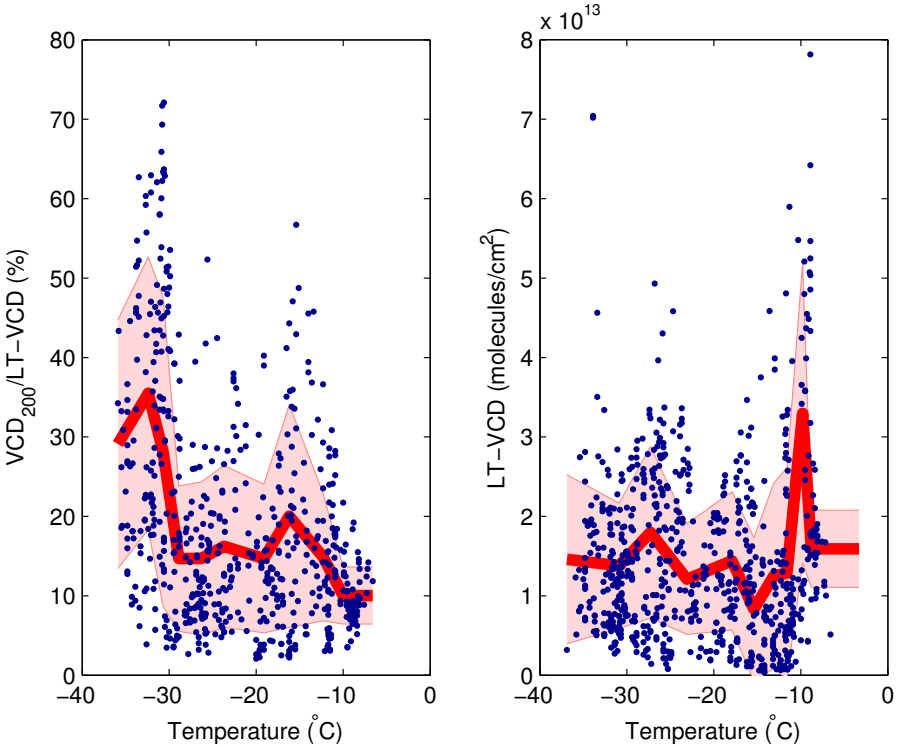

Figure 10. The relationship between BrO and temperature. The left panel shows the percentage of BrO in the lowest 200 m vs. the near-surface temperature, while the right panel shows the LT-VCD vs. the near-surface temperature. The red line represents the mean, calculated from deciles on the x axis, while the shaded region represents one standard deviation. In the left panel, LT-VCD values below 5×10^{12} molecules cm^{-2} are eliminated to avoid calculating percentages from near zero amounts of BrO.

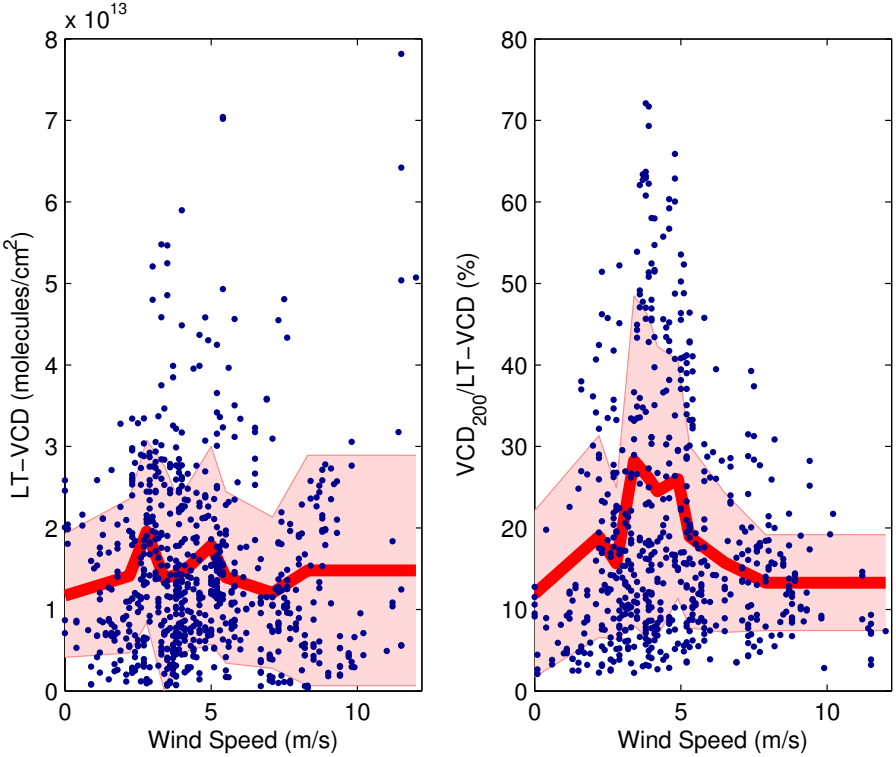

Figure 11. The left panel shows the relationship between the BrO LT-VCD and wind speed, while the right panel shows percentage of BrO in the lowest 200 m vs. the wind speed. In both cases, the red line represents the mean as a function of wind speed, calculated from deciles on the x axis, while the shaded region represents one standard deviation.

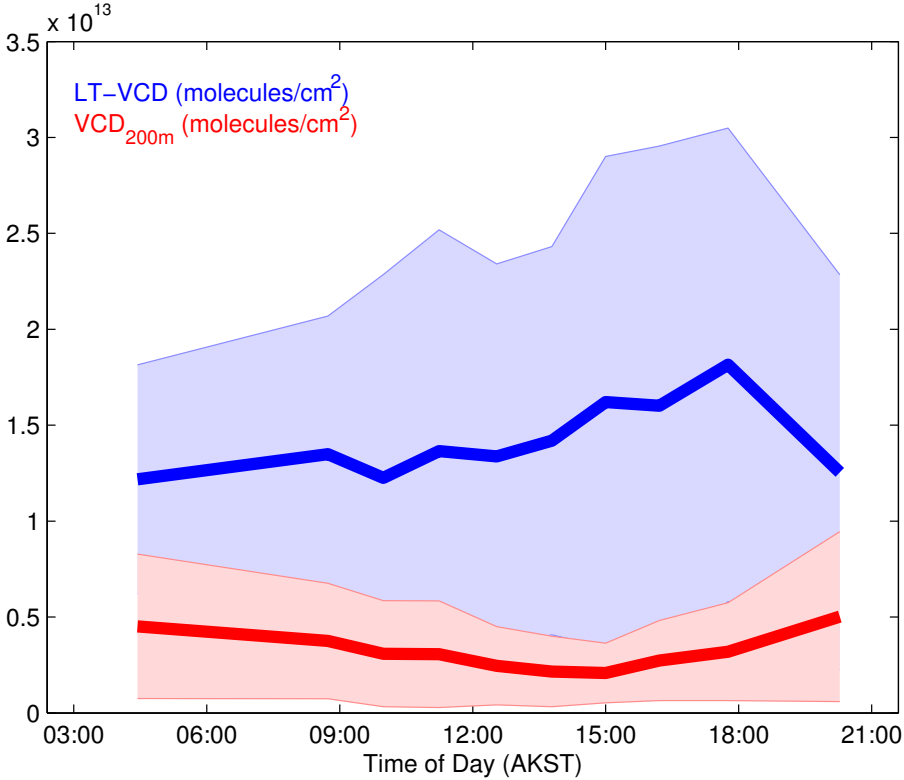

Figure 12. The diurnal cycling of the BrO LT-VCD (blue) and $VCD_{200\,m}$ (red). The solid lines represents the mean VCD as a function of time of day, while the shaded region represents one standard deviation. The shaded regions are symmetric about the mean in both cases, however the cycling of the $VCD_{200\,m}$ is overlain on the cycling of the LT-VCD, partially obscuring the standard deviation of the LT-VCD.

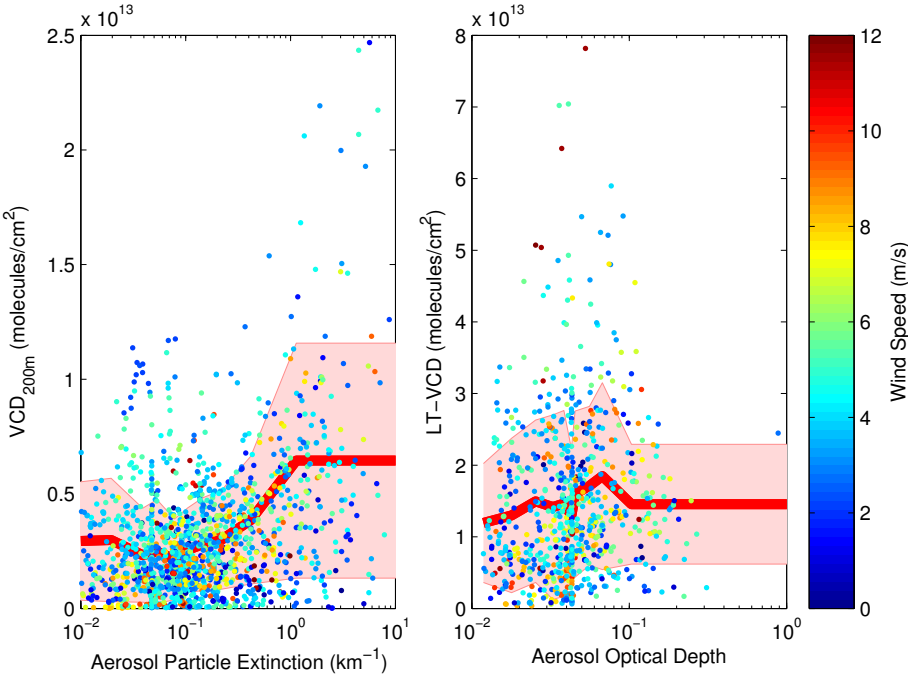

Figure 13. The left panel shows the relationship between the BrO $VCD_{200\,m}$ and the near-surface aerosol particle extinction. The right panel shows the relationship between the BrO LT-VCD and the aerosol optical depth. In both plots the x axis is a log scale. The red line represents the mean VCD, calculated from deciles on the x axis, while the shaded region represents one standard deviation. In both cases, the coloration indicates the wind speed.